Temperature-dependent resistivity in bilayer graphene due to flexural phonons

H. Ochoa,[1] Eduardo V. Castro,[1,2] M. I. Katsnelson,[3] and F. Guinea[1]
[1]*Instituto de Ciencia de Materiales de Madrid (CSIC), Sor Juana Inés de la Cruz 3, ES-28049 Madrid, Spain*
[2]*Centro de Física do Porto, Rua do Campo Alegre 687, PT-4169-007 Porto, Portugal*
[3]*Radboud University Nijmegen, Institute for Molecules and Materials, NL-6525 AJ Nijmegen, The Netherlands*
(Received 14 February 2011; published 14 June 2011)

We have studied electron scattering by out-of-plane (flexural) phonons in doped suspended bilayer graphene. We have found the bilayer membrane to follow the qualitative behavior of the monolayer cousin. In the bilayer, a different electronic structure combine with a different electron-phonon coupling to give the same parametric dependence in resistivity and, in particular, the same temperature (T) behavior. In parallel with the single layer, flexural phonons dominate the phonon contribution to resistivity in the absence of strain, where a density-independent mobility is obtained. This contribution is strongly suppressed by tension, and in-plane phonons become the dominant contribution in strained samples. Among the quantitative differences, an important one has been identified: room-temperature mobility in bilayer graphene is substantially higher than in monolayer graphene. The origin of quantitative differences has been unveiled.

DOI: 10.1103/PhysRevB.83.235416 PACS number(s): 72.10.Di, 72.80.Vp, 63.22.Rc

I. INTRODUCTION

Bilayer graphene continues to attract a great deal of attention because of both fascinating fundamental physics[1] and possible applications.[2] Recent realization of suspended monolayer[3,4] and bilayer[1] graphene samples made possible a direct probe of the intrinsic, unusual properties of these systems. In particular, intrinsic scattering mechanisms limiting mobility may now be unveiled.[5] It has been recently shown that, in suspended nonstrained monolayer graphene, room-temperature mobility is limited to values observed for samples on substrate due to scattering by out-of-plane, i.e., *flexural*, acoustic phonons.[6] This limitation can, however, be avoided by applying tension. Bilayer graphene has a different low-energy electronic behavior as well as different electron-phonon coupling. It is then natural to wonder what the situation is in the bilayer regarding electron scattering by acoustic phonons and, in particular, by flexural phonons (FPs).

In this paper, the T-dependent resistivity due to scattering by both acoustic in-plane phonons and FPs in doped, suspended bilayer graphene, has been investigated. We have found the bilayer membrane to follow the qualitative behavior of the monolayer parent.[6,7] Explicitly, at experimentally relevant T, the nonstrained samples show quadratic in T resistivity with logarithmic correction $\varrho \sim T^2 \ln(T)$ and constant mobility. Electron scattering by two FPs gives the main contribution to the resistivity in this case, and is responsible for the T^2 dependence. Suspended samples may also be under strain either due to the charging gate[8] or due to the experimental procedure to get suspended samples, or even by applying strain in a controlled way.[9,10] Under uniaxial or isotropic strain u, the T dependence of resistivity due to FPs becomes quartic at high strain $u \gg u^*$, $\varrho \sim T^4/u^3$, and quadratic at low strain $u \ll u^*$, $\varrho \sim T^2/u$, where $u^* \approx 10^{-4} T[\mathrm{K}]$. These contributions are weaker than those coming from scattering by in-plane phonons, and in strained samples, the latter dominate resistivity, as has been found for monolayer graphene.[6] An interesting quantitative difference with respect to suspended monolayer graphene has been found. In the latter, room-temperature mobility μ is limited to values obtained for samples on substrate due to FPs, $\mu \sim 1\ \mathrm{m}^2/(\mathrm{Vs})$.[6] In bilayer graphene, quantitative differences in electron-phonon coupling and elastic constants lead to room-temperature enhanced $\mu \sim 10 - 20\ \mathrm{m}^2/(\mathrm{Vs})$, even in nonstrained samples.

The paper is organized as follows. In Sec. II, we introduce long-wavelength acoustic phonons in the framework of elasticity theory. We show how the dispersion relation of FPs is affected by the presence of tension over the sample. Then, we review the electronic low-energy description of bilayer graphene and deduce the electron-phonon coupling within this approach in Sec. III. The variational approach used in order to study the T-dependent resistivity due to scattering by in-plane and FPs and a summary of our results in different regimes of T and strain are presented in Sec. IV. Section V is devoted to discuss the implications of these results, the differences between monolayer and bilayer graphene, and some experimental consequences. Finally, we expose our conclusions in Sec. VI. Some technical aspects are treated in detail in appendices. In Appendix A, we present the collision integral due to scattering by acoustic phonons, and its linearized form is derived. Details on the calculation of the resistivity using the variational method are given in Appendix B.

II. ACOUSTIC PHONONS

At long wavelengths, the elastic behavior of monolayer graphene is well approximated by that of an isotropic continuum membrane,[11,12] the free energy of which reads as[13,14]

$$\mathcal{F} = \frac{1}{2}\kappa \int dx\, dy (\nabla^2 h)^2 + \frac{1}{2}\int dx\, dy \left(\lambda u_{ii}^2 + 2\mu u_{ij}^2\right). \quad (1)$$

The first and second terms in Eq. (1) represent the bending and stretching energies, respectively. Summation over indices is assumed. In-plane distortions are denoted by $\mathbf{u}(\mathbf{r})$ and out-of-plane by $h(\mathbf{r})$, with $\mathbf{r} = (x, y)$, such that the new position is $\vec{X}(\mathbf{r}) = (x, y, 0) + [u_x(\mathbf{r}), u_y(\mathbf{r}), h(\mathbf{r})]$. To lowest order in

gradients of the deformations, the strain tensor appearing in Eq. (1) is

$$u_{ij} = \tfrac{1}{2}[\partial_i u_j + \partial_j u_i + (\partial_i h)(\partial_j h)], \tag{2}$$

and, owing to the same argument, the factor $\sqrt{g} = \sqrt{1+|\nabla h|^2}$ in the measure is neglected. The parameter κ is the bending rigidity and λ and μ are in-plane elastic constants. Typical parameters for graphene are $\kappa \approx 1$ eV and $\mu \simeq 3\lambda \approx 9$ eV Å^{-2},[12,15,16] with mass density $\rho = 7.6 \times 10^{-7}$ kg/m^2.

In the case of bilayer graphene, as long as we are not at too high T to excite optical phonons, we may, from the elastic point of view, regard bilayer graphene as a thick membrane with mass density and elastic constants twice as high as those for the single layer.[17]

The dynamics of the displacement fields is studied here in the harmonic approximation by introducing the Fourier series $\mathbf{u}(\mathbf{r}) = \mathcal{V}^{-\frac{1}{2}} \sum_{\mathbf{q}} \mathbf{u}_{\mathbf{q}} e^{i\mathbf{q}\cdot\mathbf{r}}$ and $h(\mathbf{r}) = \mathcal{V}^{-\frac{1}{2}} \sum_{\mathbf{q}} h_{\mathbf{q}} e^{i\mathbf{q}\cdot\mathbf{r}}$, where $\mathcal{V}$ is the volume of the system.

A. In-plane phonons

The decoupled in-plane phonon modes are obtained in the usual way by changing to longitudinal $u^L_{\mathbf{q}} = \mathbf{u}_{\mathbf{q}} \cdot \mathbf{q}/q$ and transverse $u^T_{\mathbf{q}} = \mathbf{u}_{\mathbf{q}} \cdot (\hat{e}_z \times \mathbf{q}/q)$ displacement fields. The dispersion relations have the usual linear behavior in momentum and are given by

$$\begin{aligned} \omega^L_{\mathbf{q}} &= v_L q, \\ \omega^T_{\mathbf{q}} &= v_T q, \end{aligned} \tag{3}$$

with $v_L = \sqrt{\frac{2\mu+\lambda}{\rho}}$ and $v_T = \sqrt{\frac{\mu}{\rho}}$. Typical values for monolayer and bilayer graphene are $v_L \simeq 2.1 \times 10^4$ m/s and $v_T \simeq 1.4 \times 10^4$ m/s.

B. Flexural phonons

1. Nonstrained case

The quadratic behavior in out-of-plane displacements of the strain tensor in Eq. (2) implies that FP modes are driven by the bending rigidity term. The resulting FP dispersion relation is quadratic, i.e.,[11,18]

$$\omega^F_{\mathbf{q}} = \alpha q^2, \tag{4}$$

with $\alpha = \sqrt{\frac{\kappa}{\rho}}$. The typical value is $\alpha \simeq 4.6 \times 10^{-7}$ m^2/s.

2. Strained case

Suspended samples may be under tension either due to the load imposed by the back gate or as a result of the fabrication process, or both. The case of a clamped graphene membrane hanging over a trench of size L, relevant for conventional two-contacts measurements in suspended samples, has been considered in Ref. 19.

Once the membrane is under tension, a static deformation configuration is expected at equilibrium. The phonon modes may be obtained by assuming that both in-plane $\mathbf{u}(\mathbf{r})$ and flexural $h(\mathbf{r})$ fields have dynamic components that add to their static background: $\mathbf{u}(\mathbf{r}) = \mathbf{u}_{st}(\mathbf{r}) + \mathbf{u}_{dyn}(\mathbf{r})$ and $h(\mathbf{r}) = h_{st}(\mathbf{r}) + h_{dyn}(\mathbf{r})$. For the case of the clamped membrane considered in Ref. 19, we have $\mathbf{u}_{st}(\mathbf{r}) = [u_{x,st}(x),0]$ with $u_{x,st}(x)$ a linear function of x, while $h_{st}(x)$ may be approximated by a parabola.

Let us consider the general static displacement vector field $\mathbf{d}_{st}(\mathbf{r}) = [u_{x,st}(\mathbf{r}),u_{y,st}(\mathbf{r}),h_{st}(\mathbf{r})]$ and the associated strain tensor $u_{ij,st}(\mathbf{r}) = \frac{1}{2}(\partial_i u_{j,st} + \partial_j u_{i,st} + \partial_i h_{st}\partial_j h_{st})$. In-plane phonons are not affected by the static component, but the FP dispersion changes considerably. This is a consequence of new harmonic terms appearing due to coupling between in-plane static deformation and out-of-plane vibrations in the full strain tensor in Eq. (2). The resulting FP dispersion relation may be obtained using a *local approximation* expected to hold for $L \gg \ell = v_F\tau \gg k_F^{-1}$, where v_F is the Fermi velocity, k_F the Fermi momentum, and τ a characteristic collision time. The result reads as

$$\omega^F_{\mathbf{q}}(\mathbf{r}) = q\sqrt{\frac{\kappa}{\rho}q^2 + u_{ii,st}(\mathbf{r})\frac{\lambda}{\rho} + u_{ij,st}(\mathbf{r})\frac{2\mu}{\rho}\frac{q_i q_j}{q^2}}. \tag{5}$$

For the particular case of isotropic strain where $u_{xx} = u_{yy}$ and $u_{xy} = 0$, the dispersion relation can be cast in the form

$$\omega^F_{\mathbf{q}}(\mathbf{r}) = q\sqrt{\frac{\kappa}{\rho}q^2 + u_{ii,st}(\mathbf{r})\frac{\lambda+\mu}{\rho}}. \tag{6}$$

Here, we will give particular emphasis to the clamped membrane case where the FP dispersion is given by

$$\omega^F_{\mathbf{q}} = q\sqrt{\frac{\kappa}{\rho}q^2 + \bar{u}\frac{\lambda+2\mu}{\rho} - \bar{u}\frac{2\mu}{\rho}\sin^2\phi_{\mathbf{q}}}, \tag{7}$$

with $\bar{u} \equiv u_{xx}$ and $\phi_{\mathbf{q}} = \arctan(q_y/q_x)$. In order to keep the problem within analytical treatment, we will use an effective isotropic dispersion relation, obtained by dropping the angular dependence contribution

$$\omega^F_{\mathbf{q}} \simeq q\sqrt{\alpha^2 q^2 + \bar{u}v_L^2}. \tag{8}$$

Since we are mainly interested in transport, such an approximation has the advantage that backward scattering is still correctly accounted for.

III. ELECTRON-PHONON INTERACTION

A. Low-energy description for bilayer graphene

At low energies, the two-band effective model provides a good approximate description for π electrons in bilayer graphene.[11] The 2×2 Hamiltonian can be cast in the form $\mathcal{H}_{\text{eff}} = \sum_{\mathbf{k}} \psi_{\mathbf{k}} \mathcal{H}_{\mathbf{k}} \psi_{\mathbf{k}}$, with

$$\mathcal{H}_{\mathbf{k}} = \frac{\hbar^2}{2m}\begin{pmatrix} 0 & (k_x - ik_y)^2 \\ (k_x + ik_y)^2 & 0 \end{pmatrix}, \tag{9}$$

where the two-component spinor $\psi^\dagger_{\mathbf{k}} = [a^\dagger_{\mathbf{k}}, b^\dagger_{\mathbf{k}}]$ stems from the two sublattices not connected by the interlayer hopping $t_\perp \approx 0.3$ eV. The coupling $t_\perp$ between layers sets the effective mass $2m = t_\perp/v_F^2$, with $v_F \approx 10^6$ m/s the Fermi velocity in monolayer graphene. Equation (9) is valid at valley K, and at valley K' we have $\mathcal{H}_{\mathbf{k}} \to \mathcal{H}^T_{\mathbf{k}}$. Here, we are interested in electron scattering processes induced by emission or

absorption of long-wavelength acoustic phonons and, hence, intervalley scattering is not allowed. Thus, we may concentrate on one valley only. The Hamiltonian can be diagonalized introducing the rotated operators

$$d_{\mathbf{k}} = \frac{1}{\sqrt{2}} \begin{pmatrix} e^{i\theta_{\mathbf{k}}} & e^{-i\theta_{\mathbf{k}}} \\ e^{i\theta_{\mathbf{k}}} & -e^{-i\theta_{\mathbf{k}}} \end{pmatrix} \psi_{\mathbf{k}}, \tag{10}$$

where $\theta_{\mathbf{k}} = \arctan(k_y/k_x)$, with $d_{\mathbf{k}}^\dagger = [e_{\mathbf{k}}^\dagger, h_{\mathbf{k}}^\dagger]$ defined such that $e_{\mathbf{k}}^\dagger$ stands for electronlike (positive energy) excitations and $h_{\mathbf{k}}^\dagger$ for holelike (negative energy) excitations, from which we get

$$\mathcal{H} = \sum_{\mathbf{k}} \varepsilon(\mathbf{k})[e_{\mathbf{k}}^\dagger e_{\mathbf{k}} - h_{\mathbf{k}}^\dagger h_{\mathbf{k}}], \tag{11}$$

with $\varepsilon(\mathbf{k}) = \hbar^2 k^2/(2m)$.

In this paper, we will compare the results obtained for bilayer graphene with those valid in monolayer graphene. The latter is described using the effective Dirac-type Hamiltonian,[11] which holds in the low-energy sector in which we are interested here.

B. Coupling between electrons and phonons

The coupling between electrons and the vibrations of the underlying lattice either in bilayer or monolayer graphene has two main sources. Long-wavelength acoustic phonons induce an effective local potential called deformation potential and proportional to the local contraction or dilation of the lattice[11]

$$V_1(\mathbf{r}) = g_0 u_{ii}(\mathbf{r}),$$

where g_0 is the bare deformation potential constant, the value of which is in the range $g_0 \approx 20$–30 eV.[20] The respective interaction Hamiltonian is diagonal in sublattice indices and reads as

$$\mathcal{H}_1 = \sum_{\mathbf{k}} \psi_{\mathbf{k}}^\dagger [V_1(\mathbf{k},\mathbf{k}')\mathbb{I}]\psi_{\mathbf{k}'}, \tag{12}$$

where $\mathbb{I}$ is the 2×2 identity matrix and $V_1(\mathbf{k},\mathbf{k}')$ is the Fourier transform of the deformation potential

$$V_1(\mathbf{k},\mathbf{k}') = \mathcal{V}^{-1} g_0 \int d\mathbf{r}\, e^{i(\mathbf{k}'-\mathbf{k})\cdot\mathbf{r}} u_{ii}(\mathbf{r}). \tag{13}$$

Equation (12) is valid both for monolayer and bilayer graphene. Since we are interested in doped systems, we take into account screening by substituting $V_1(\mathbf{k},\mathbf{k}')$ with $V_1(\mathbf{k},\mathbf{k}')/\epsilon(\mathbf{k}-\mathbf{k}')$, where we take a Thomas-Fermi–type dielectric function

$$\epsilon(\mathbf{q}) = 1 + \frac{e^2 \mathcal{D}(E_F)}{2\epsilon_0 q}, \tag{14}$$

and $\mathcal{D}(E_F)$ is the density of states at the Fermi energy, which is given by $\mathcal{D}(E_F) = \frac{2E_F}{\pi\hbar^2 v_F^2} = \frac{2k_F}{\pi\hbar v_F}$ in the case of monolayer graphene and by $\mathcal{D}(E_F) = \frac{t_\perp}{\pi\hbar^2 v_F^2}$ in the case of bilayer graphene.

It is convenient to define $g \equiv g_0/\epsilon(k_F)$ for single-layer graphene, which gives a density-independent screened deformation potential

$$g \approx \frac{g_0}{e^2/(\pi\epsilon_0\hbar v_F)} \approx \frac{g_0}{8.75} \approx 2\text{–}3.5 \text{ eV}. \tag{15}$$

Note that the value just obtained is in complete agreement with recent *ab initio* calculations, which give $g \approx 3$ eV.[21] It will become clear in Sec. IV C 1 that g, as defined in Eq. (15), is the relevant deformation potential electron-phonon parameter in single-layer graphene. For bilayer graphene, $g(q) = g_0/\epsilon(q)$ gives

$$g(k_F) \approx \frac{g_0}{e^2 t_\perp/(2\pi\epsilon_0\hbar^2 v_F^2 k_F)} \approx \frac{g_0}{11.25}\sqrt{n} \approx (2\text{–}3)\sqrt{n} \text{ eV}, \tag{16}$$

with n in 10^{12} cm^{-2}. We may then write a q-dependent deformation potential electron-phonon parameter, which has the form $g_M(q) = gq/k_F$ for monolayer graphene and $g_B(q) = g2\hbar v_F q/t_\perp$ for bilayer graphene.

Phonons can also couple to electrons in monolayer and bilayer graphene by changes in bond length and bond angle between carbon atoms. In this case, the electron-phonon interaction can be written as due to an effective gauge field[22–25]

$$e\mathbf{A}_{\text{elastic}} = \frac{\beta}{a}\left[\frac{1}{2}(u_{xx} - u_{yy}), \quad -u_{xy}\right],$$

where $\beta \approx -\partial \log t/\partial \log a \sim 2$–$3$,[20] with t the in-plane nearest-neighbor hopping parameter and a the carbon-carbon distance ($t_0 \approx 3$ eV and $a_0 \approx 1.4$ Å). In the case of bilayer graphene, the resulting interaction Hamiltonian is obtained by introducing the gauge potential into Eq. (9), following the minimal coupling prescription, and keeping only first-order terms in electron-phonon coupling. Then, we arrive at

$$\mathcal{H}_2 = \frac{\hbar}{2m} \sum_{\mathbf{k},\mathbf{k}'} \psi_{\mathbf{k}}^\dagger \begin{bmatrix} 0 & (\pi_{\mathbf{k}}^- + \pi_{\mathbf{k}'}^-)A_{\mathbf{k},\mathbf{k}'}^- \\ (\pi_{\mathbf{k}}^+ + \pi_{\mathbf{k}'}^+)A_{\mathbf{k},\mathbf{k}'}^+ & 0 \end{bmatrix} \psi_{\mathbf{k}'}, \tag{17}$$

where $\pi_{\mathbf{k}}^\pm = ke^{\pm i\theta_{\mathbf{k}}}$, $A_{\mathbf{k},\mathbf{k}'}^\pm = V_{2,x}(\mathbf{k},\mathbf{k}') \pm i V_{2,y}(\mathbf{k},\mathbf{k}')$, and the vector $\mathbf{V}_2 = (V_{2,x}, V_{2,y})$ is defined as

$$V_{2,x}(\mathbf{k},\mathbf{k}') = \frac{\hbar\beta}{a}\mathcal{V}^{-1}\int d\mathbf{r}\, e^{i(\mathbf{k}'-\mathbf{k})\cdot\mathbf{r}} \frac{1}{2}[u_{xx}(\mathbf{r}) - u_{yy}(\mathbf{r})],$$
$$V_{2,y}(\mathbf{k},\mathbf{k}') = -\frac{\hbar\beta}{a}\mathcal{V}^{-1}\int d\mathbf{r}\, e^{i(\mathbf{k}'-\mathbf{k})\cdot\mathbf{r}} u_{xy}(\mathbf{r}). \tag{18}$$

An estimate of the electron-phonon coupling strength due to V_2 is given by $k_F\hbar^2\beta/(ma) \approx (8\text{–}12)\sqrt{n}$ eV, with n in 10^{12} cm^{-2}. In the case of single-layer graphene, the resulting interaction Hamiltonian reads as

$$\mathcal{H}_2 = v_F \sum_{\mathbf{k},\mathbf{k}'} \psi_{\mathbf{k}}^\dagger \boldsymbol{\sigma}\cdot\mathbf{V}_2(\mathbf{k},\mathbf{k}')\psi_{\mathbf{k}'}, \tag{19}$$

where $\boldsymbol{\sigma} = (\sigma_x, \sigma_y)$ is the vector of Pauli matrices, and the two-component spinor $\psi_{\mathbf{k}}^\dagger = [a_{\mathbf{k}}^\dagger, b_{\mathbf{k}}^\dagger]$ is reminiscent of the two sublattices of the honeycomb lattice. An estimate of the respective electron-phonon coupling strength is given by $v_F\hbar\beta/a \approx 10$–$15$ eV.

The electron-phonon interaction Hamiltonian is the sum of the two terms shown above, $H_{e\text{-}p} = \mathcal{H}_1 + \mathcal{H}_2$. Phonons enter through the strain tensor u_{ij}, which we have seen can be written in terms of static and dynamic components, the static ones being zero for zero load. There are purely static terms that do not contribute to electron-phonon scattering and will be dropped (see Ref. 19). By quantizing the dynamic part of

the displacement fields,[26] and introducing usual destruction and creation operators $a^{\nu}_{\mathbf{q}}$ and $(a^{\nu}_{\mathbf{q}})^{\dagger}$ for in-plane phonons $\mathbf{q}$ and polarization $\nu = L,T$, we can write the $\mathbf{q}$ component of the in-plane displacement as

$$u^{L/T}_{\mathbf{q}} = \sqrt{\frac{\hbar}{2\rho\omega^{\nu}_{\mathbf{q}}}}\left[a^{L/T}_{\mathbf{q}} + \left(a^{L/T}_{-\mathbf{q}}\right)^{\dagger}\right]. \tag{20}$$

For FPs, we introduce the bosonic fields $a^{F}_{\mathbf{q}}$ and $(a^{F}_{\mathbf{q}})^{\dagger}$, and write the $\mathbf{q}$ component of the out-of-plane displacement as

$$h_{\mathbf{q}} = \sqrt{\frac{\hbar}{2\rho\omega^{F}_{\mathbf{q}}}}\left[a^{F}_{\mathbf{q}} + \left(a^{F}_{-\mathbf{q}}\right)^{\dagger}\right]. \tag{21}$$

The electron-phonon interaction Hamiltonian may then be written either in monolayer or bilayer graphene as

$$H_{e\text{-}p} = \sum_{\mathbf{k},\mathbf{k}'}(a^{\dagger}_{\mathbf{k}}a_{\mathbf{k}'} + b^{\dagger}_{\mathbf{k}}b_{\mathbf{k}'})\left\{\sum_{\nu,\mathbf{q}} V^{\nu}_{1,\mathbf{q}}\left[a^{\nu}_{\mathbf{q}} + \left(a^{\nu}_{-\mathbf{q}}\right)^{\dagger}\right]\delta_{\mathbf{k}',\mathbf{k}-\mathbf{q}} + \sum_{\mathbf{q},\mathbf{q}'} V^{F}_{1,\mathbf{q},\mathbf{q}'}\left[a^{F}_{\mathbf{q}} + \left(a^{F}_{-\mathbf{q}}\right)^{\dagger}\right]\left[a^{F}_{\mathbf{q}'} + \left(a^{F}_{-\mathbf{q}'}\right)^{\dagger}\right]\delta_{\mathbf{k}',\mathbf{k}-\mathbf{q}-\mathbf{q}'}\right\}$$
$$+ \sum_{\mathbf{k},\mathbf{k}'}\left\{\sum_{\nu,\mathbf{q}} V^{\nu}_{2,\mathbf{q}}a^{\dagger}_{\mathbf{k}}b_{\mathbf{k}'}\left[a^{\nu}_{\mathbf{q}} + \left(a^{\nu}_{-\mathbf{q}}\right)^{\dagger}\right]\delta_{\mathbf{k}',\mathbf{k}-\mathbf{q}} + \sum_{\mathbf{q},\mathbf{q}'} V^{F}_{2,\mathbf{q},\mathbf{q}'}a^{\dagger}_{\mathbf{k}}b_{\mathbf{k}'}\left[a^{F}_{\mathbf{q}} + \left(a^{F}_{-\mathbf{q}}\right)^{\dagger}\right]\left[a^{F}_{\mathbf{q}'} + \left(a^{F}_{-\mathbf{q}'}\right)^{\dagger}\right]\delta_{\mathbf{k}',\mathbf{k}-\mathbf{q}-\mathbf{q}'} + \text{H.c.}\right\}. \tag{22}$$

For monolayer graphene, the matrix elements read as

$$V^{L}_{1,\mathbf{q}} = \frac{g_0}{\epsilon(q)}iq\sqrt{\frac{\hbar}{2\mathcal{V}\rho\omega^{L}_{\mathbf{q}}}},$$
$$V^{F}_{1,\mathbf{q},\mathbf{q}'} = -\frac{g_0}{\epsilon(|\mathbf{q}+\mathbf{q}'|)}qq'\cos(\phi_{\mathbf{q}} - \phi_{\mathbf{q}'})\frac{\hbar}{4\mathcal{V}\rho\sqrt{\omega^{F}_{\mathbf{q}}\omega^{F}_{\mathbf{q}'}}},$$
$$V^{F}_{1,\mathbf{q}} = \frac{g_0}{\epsilon(q)}iq_i\partial_i h_{st}\sqrt{\frac{\hbar}{2\mathcal{V}\rho\omega^{F}_{\mathbf{q}}}},$$
$$V^{L}_{2,\mathbf{q}} = \frac{\hbar v_F\beta}{2a}iqe^{i2\phi_{\mathbf{q}}}\sqrt{\frac{\hbar}{2\mathcal{V}\rho\omega^{L}_{\mathbf{q}}}}, \tag{23}$$
$$V^{T}_{2,\mathbf{q}} = -\frac{\hbar v_F\beta}{2a}qe^{i2\phi_{\mathbf{q}}}\sqrt{\frac{\hbar}{2\mathcal{V}\rho\omega^{T}_{\mathbf{q}}}},$$
$$V^{F}_{2,\mathbf{q},\mathbf{q}'} = -\frac{\hbar v_F\beta}{4a}qq'e^{i(\phi_{\mathbf{q}}-\phi_{\mathbf{q}'})}\frac{\hbar}{2\mathcal{V}\rho\sqrt{\omega^{F}_{\mathbf{q}}\omega^{F}_{\mathbf{q}'}}},$$
$$V^{F}_{2,\mathbf{q}} = \frac{\hbar v_F\beta}{2a}iq\left[e^{i\phi_{\mathbf{q}}}\partial_x h_{st} + e^{-i\phi_{\mathbf{q}}}\partial_y h_{st}\right]\sqrt{\frac{\hbar}{2\mathcal{V}\rho\omega^{F}_{\mathbf{q}}}},$$

with $V^{T}_{1,\mathbf{q}} = 0$ (see also Refs. 7 and 18), and where we have again used the local approximation. In the case of bilayer graphene, only the matrix elements for the gauge potential change, becoming dependent on fermionic momenta $\mathbf{k}$ and $\mathbf{k}'$. As can be seen by comparing Eqs. (17) and (19), they take exactly the same form as in Eq. (23) with the replacement $v_F \to \hbar(\pi_{\mathbf{k}} + \pi_{\mathbf{k}'})/(2m)$.

IV. TEMPERATURE-DEPENDENT RESISTIVITY

Our aim here is to study the T-dependent resistivity in suspended bilayer graphene as a result of the electron-phonon interaction derived above. We assume the doped regime $E_F \gg \hbar/\tau$, where $1/\tau$ is the characteristic electronic scattering rate (due to phonons, disorder, etc). The doped regime immediately implies $k_F^{-1} \ll v_F\tau \equiv l$, where l is the characteristic mean-free path, thus justifying the use of Boltzmann transport theory (even though graphene's quasiparticles are chiral, the semiclassical approach still holds away from the Dirac point [27,28]).

A. The variational approach

The Boltzmann equation is an integrodifferentialequation for the steady-state probability distribution $f_{\mathbf{k}}$.[29] It can be generally written as

$$\dot{\mathbf{r}}\cdot\nabla_{\mathbf{r}}f_{\mathbf{k}} + \dot{\mathbf{k}}\cdot\nabla_{\mathbf{k}}f_{\mathbf{k}} = \dot{f}_{\mathbf{k}}\big|_{\text{scatt}}, \tag{24}$$

where the terms on the left-hand side are due to, respectively, *diffusion* and *external fields*, while on the right-hand side, *scattering* provides the required balance at the steady state. (See Appendix A for an explicit form of $\dot{f}_{\mathbf{k}}\big|_{\text{scatt}}$ in the case under study.) The Boltzmann equation is quite intractable in practice, and its linearized version is used instead:

$$\dot{\mathbf{r}}\cdot\nabla_{\mathbf{r}}f^{(0)}_{\mathbf{k}} + \dot{\mathbf{k}}\cdot\nabla_{\mathbf{k}}f^{(0)}_{\mathbf{k}} = \delta\dot{f}_{\mathbf{k}}\big|_{\text{scatt}}, \tag{25}$$

where $\delta\dot{f}_{\mathbf{k}}\big|_{\text{scatt}}$ is the linearized collision integral. (See Appendix A for an explicit form of $\delta\dot{f}_{\mathbf{k}}\big|_{\text{scatt}}$ in the case under study.) By expanding the distribution probability around its equilibrium value $f^{(0)}_{\mathbf{k}} = 1/\{\exp[(\varepsilon_{\mathbf{k}} - \mu)/k_BT] + 1\}$,

$$f_{\mathbf{k}} = f^{(0)}_{\mathbf{k}} - \frac{\partial f^{(0)}_{\mathbf{k}}}{\partial\varepsilon_{\mathbf{k}}}\Phi_{\mathbf{k}}, \tag{26}$$

and using the equilibrium property that $\dot{f}^{(0)}_{\mathbf{k}}\big|_{\text{scatt}} = 0$, it can be seen that $\delta\dot{f}_{\mathbf{k}}\big|_{\text{scatt}}$ is linear in $\Phi_{\mathbf{k}}$, and that it can be written as a linear application in terms of the linear scattering operator $P_{\mathbf{k}}$:

$$\delta\dot{f}_{\mathbf{k}}\big|_{\text{scatt}} = P_{\mathbf{k}}\Phi_{\mathbf{k}} \equiv -\sum_{\mathbf{k}_1,\ldots,\mathbf{k}_n}\mathcal{P}_{\mathbf{k},\mathbf{k}_1,\ldots,\mathbf{k}_n} \times(\Phi_{\mathbf{k}} \pm \Phi_{\mathbf{k}_1},\ldots,\pm\Phi_{\mathbf{k}_n}), \tag{27}$$

where $\mathcal{P}_{\mathbf{k},\mathbf{k}_1,\ldots,\mathbf{k}_n}$ is a generalized transition rate per unit energy.[29] (See Appendix A for an explicit form of $\mathcal{P}_{\mathbf{k},\mathbf{k}_1,\ldots,\mathbf{k}_n}$ in the case under study.) By writing the linearized Boltzmann equation (25) in the form

$$X_{\mathbf{k}} = P_{\mathbf{k}}\Phi_{\mathbf{k}},$$

and defining the inner products

$$\langle \Phi, X \rangle = \sum_{\mathbf{k}} \Phi_{\mathbf{k}} \left(\dot{\mathbf{r}} \cdot \nabla_{\mathbf{r}} f_{\mathbf{k}}^{(0)} + \dot{\mathbf{k}} \cdot \nabla_{\mathbf{k}} f_{\mathbf{k}}^{(0)} \right) \tag{28}$$

and

$$\begin{aligned} \langle \Phi, P\Phi \rangle &= \sum_{\mathbf{k},\mathbf{k}_1,\ldots,\mathbf{k}_n} \Phi_{\mathbf{k}} \mathcal{P}_{\mathbf{k},\mathbf{k}_1,\ldots,\mathbf{k}_n} (\Phi_{\mathbf{k}} \pm \Phi_{\mathbf{k}_1}, \ldots, \pm \Phi_{\mathbf{k}_n}) \\ &= \frac{1}{(n+1)} \sum_{\mathbf{k},\mathbf{k}_1,\ldots,\mathbf{k}_n} (\Phi_{\mathbf{k}} \pm \Phi_{\mathbf{k}_1}, \ldots, \pm \Phi_{\mathbf{k}_n})^2 \mathcal{P}_{\mathbf{k},\mathbf{k}_1,\ldots,\mathbf{k}_n}, \end{aligned} \tag{29}$$

the *variational principle* asserts that of all functions $\Phi_{\mathbf{k}}$ satisfying $\langle \Phi, X \rangle = \langle \Phi, P\Phi \rangle$, the solution of the linearized Boltzmann equation gives to the quantity $\langle \Phi, P\Phi \rangle / \{\langle \Phi, X \rangle\}^2$ its *minimum* value.[29] In particular, the resistivity ϱ can be written as

$$\varrho = \frac{1}{g_d} \frac{\langle \Phi, P\Phi \rangle}{\{\langle \Phi, X(E=1, \nabla_{\mathbf{r}} f^{(0)} = 0) \rangle\}^2}, \tag{30}$$

being thus expected to be a *minimum* for the right solution,[29] where g_d is the system's degeneracy (for monolayer and bilayer graphene, it is $g_d = g_s g_v = 4$ due to spin and valley degeneracies). The quantity $X(E = 1, \nabla_{\mathbf{r}} f^{(0)} = 0)$ refers to the left-hand side of Eq. (25) in a unit electric field and no spatial gradients (for example, zero-temperature gradient). It is easy to show that $\langle \Phi, X \rangle = \mathbf{E} \cdot \mathbf{J}$, where

$$\mathbf{J} = \sum_{\mathbf{k}} e \mathbf{v}_{\mathbf{k}} \Phi_{\mathbf{k}} \frac{\partial f_{\mathbf{k}}^{(0)}}{\partial \varepsilon_{\mathbf{k}}}$$

is the current per nondegenerate mode (per spin and valley in monolayer and bilayer graphene). The quantity $\{\langle \Phi, X(E = 1, \nabla_{\mathbf{r}} f^{(0)} = 0) \rangle\}^2$ is therefore nothing but $\mathcal{V} \mathbf{j}^2$, where $\mathbf{j} = \mathbf{J}/\mathcal{V}$ is the current density.

A well-known solution to the Boltzmann equation exists when scattering is elastic, the Fermi surface isotropic, and the transition rate can be written as $\mathcal{P}_{\mathbf{k},\mathbf{k}'} = \mathcal{P}(k, \theta_{\mathbf{k},\mathbf{k}'})$, where $\theta_{\mathbf{k},\mathbf{k}'} = \theta_{\mathbf{k}} - \theta_{\mathbf{k}'}$ is the angle between $\mathbf{k}$ and $\mathbf{k}'$.[29] Under these conditions, the solution reads as

$$\Phi_{\mathbf{k}} = v_{\mathbf{k}} \cdot \left(e\mathbf{E} - \frac{\varepsilon_k}{T} \nabla T \right) \tau(k),$$

where $\tau(k)$ is the isotropic scattering rate, and we have written $\nabla_{\mathbf{r}} f_{\mathbf{k}}^{(0)} = \partial f_{\mathbf{k}}^{(0)} / \partial \varepsilon_{\mathbf{k}} \nabla T$. Clearly, the latter solution for $\Phi_{\mathbf{k}}$ can be cast in the form $\Phi_{\mathbf{k}} \propto \mathbf{k} \cdot \mathbf{u}$,[29,30] where $\mathbf{u}$ is a unit vector in the direction of the applied fields. So, in more complicated cases where there is a departure from the isotropic conditions and/or from elastic scattering, it is a good starting point to use Eq. (30) with $\Phi_{\mathbf{k}} \propto \mathbf{k} \cdot \mathbf{u}$ to get an approximate (from above) result for the resistivity. Note that the coefficient multiplying $\mathbf{k} \cdot \mathbf{u}$ is unimportant as it cancels out. This variational method is equivalent to a linear-response Kubo-Nakano-Mori approach with the perturbation inducing scattering treated in the Born approximation.[31]

Here we use the variational method just outlined to get the T-dependent resistivity in bilayer graphene (and monolayer for comparison) due to scattering by acoustic phonons. In this case, using the quasielastic approximation (see Appendix A), $\delta \dot{f}_{\mathbf{k}}\big|_{\text{scatt}}$ can indeed be cast in the form of Eq. (27), i.e.,

$$\delta \dot{f}_{\mathbf{k}}|_{\text{scatt}} = -\sum_{\mathbf{k}'} \mathcal{P}_{\mathbf{k},\mathbf{k}'} (\Phi_{\mathbf{k}} - \Phi_{\mathbf{k}'}), \tag{31}$$

where, for scattering by one in-plane phonon,

$$\mathcal{P}_{\mathbf{k},\mathbf{k}'} = \frac{2\pi}{\hbar} \sum_{\mathbf{q},\nu} w_\nu(\mathbf{q},\mathbf{k},\mathbf{k}') \omega_{\mathbf{q}}^\nu \frac{\partial n_{\mathbf{q}}}{\partial \omega_{\mathbf{q}}^\nu} \frac{\partial f_{\mathbf{k}}^{(0)}}{\partial \varepsilon_{\mathbf{k}}} \delta_{\mathbf{k},\mathbf{k}'+\mathbf{q}} \delta(\varepsilon_{\mathbf{k}} - \varepsilon_{\mathbf{k}'}), \tag{32}$$

and, for scattering by two FPs,

$$\begin{aligned} \mathcal{P}_{\mathbf{k},\mathbf{k}'} = &-\frac{2\pi}{\hbar^2} k_B T \frac{\partial f_{\mathbf{k}}^{(0)}}{\partial \varepsilon_{\mathbf{k}}} \sum_{\mathbf{q},\mathbf{q}'} w_F(\mathbf{q},\mathbf{q}',\mathbf{k},\mathbf{k}') \frac{\partial n_{\mathbf{q}}}{\partial \omega_{\mathbf{q}}^F} \frac{\partial n_{\mathbf{q}'}}{\partial \omega_{\mathbf{q}'}^F} \\ &\times \left(\frac{\omega_{\mathbf{q}}^F + \omega_{\mathbf{q}'}^F}{1 + n_{\mathbf{q}} + n_{\mathbf{q}'}} - \frac{\omega_{\mathbf{q}}^F - \omega_{\mathbf{q}'}^F}{n_{\mathbf{q}} - n_{\mathbf{q}'}} \right) \delta_{\mathbf{k},\mathbf{k}'+\mathbf{q}+\mathbf{q}'} \delta(\varepsilon_{\mathbf{k}} - \varepsilon_{\mathbf{k}'}), \end{aligned} \tag{33}$$

with $n_{\mathbf{q}} = 1/[\exp(\hbar\omega_{\mathbf{q}}/k_B T) - 1]$ the equilibrium phonon distribution. The kernel quantities $w_\nu(\mathbf{q},\mathbf{k},\mathbf{k}')$ and $w_F(\mathbf{q},\mathbf{q}',\mathbf{k},\mathbf{k}')$ are related to the matrix elements in Eq. (23) as follows (see Appendix A). For bilayer graphene,

$$\begin{aligned} w_\nu(\mathbf{q},\mathbf{k},\mathbf{k}') \approx &\left| V_{1,\mathbf{q}}^\nu \right|^2 (1 + \cos 2\theta_{\mathbf{k},\mathbf{k}'}) \\ &+ \left| \tilde{V}_{2,\mathbf{q}}^\nu \right|^2 (k^2 + k'^2 + 2kk' \cos\theta_{\mathbf{k},\mathbf{k}'}) \end{aligned} \tag{34}$$

for one-phonon processes, and a similar expression for two-phonon processes $w_F(\mathbf{q},\mathbf{q}',\mathbf{k},\mathbf{k}')$ with $V_{\mathbf{q}}^\nu \to V_{\mathbf{q},\mathbf{q}'}^F$, where $\tilde{V}_2$ means the matrix elements given in Eq. (23) for the gauge potential without the term $(\pi_{\mathbf{k}} + \pi_{\mathbf{k}'})$; for monolayer graphene, in the case of one-phonon process,

$$w_\nu(\mathbf{q},\mathbf{k},\mathbf{k}') \approx \left| V_{1,\mathbf{q}}^\nu \right|^2 (1 + \cos\theta_{\mathbf{k},\mathbf{k}'}) + \left| V_{2,\mathbf{q}}^\nu \right|^2, \tag{35}$$

with a similar expression for two-phonon processes $w_F(\mathbf{q},\mathbf{q}',\mathbf{k},\mathbf{k}')$ with $V_{\mathbf{q}}^\nu \to V_{\mathbf{q},\mathbf{q}'}^F$.

By using the setting given above, the resistivity is conveniently written as

$$\begin{aligned} \varrho &= \frac{1}{g_s g_v} \frac{\frac{1}{2} \sum_{\mathbf{k},\mathbf{k}'} (\Phi_{\mathbf{k}} - \Phi_{\mathbf{k}'})^2 \mathcal{P}_{\mathbf{k},\mathbf{k}'}}{\mathcal{V} \left| \frac{e}{\mathcal{V}} \sum_{\mathbf{k}} \Phi_{\mathbf{k}} \mathbf{v}_{\mathbf{k}} \frac{\partial f_{\mathbf{k}}^{(0)}}{\partial \varepsilon_{\mathbf{k}}} \right|^2} \\ &\approx \frac{\mathcal{V}}{8e^2} \frac{\int d\mathbf{k}\, d\mathbf{k}'\, (\mathbf{K} \cdot \mathbf{u})^2 \mathcal{P}_{\mathbf{k},\mathbf{k}'}}{\left| \int d\mathbf{k}\, \mathbf{k} \cdot \mathbf{u} \mathbf{v}_{\mathbf{k}} \frac{\partial f_{\mathbf{k}}^{(0)}}{\partial \varepsilon_{\mathbf{k}}} \right|^2}, \end{aligned} \tag{36}$$

where we changed from summation over $\mathbf{k}$ space to integration, and defined $\mathbf{K} = \mathbf{k} - \mathbf{k}'$. The integral in the denominator can be done immediately assuming $\varepsilon_F \gg k_B T$. The result reads the same for bilayer and monolayer graphene:

$$\left| \int d\mathbf{k}\, \mathbf{k} \cdot \mathbf{u} \mathbf{v}_{\mathbf{k}} \frac{\partial f_{\mathbf{k}}^{(0)}}{\partial \varepsilon_{\mathbf{k}}} \right| \approx \frac{\pi k_F^2}{\hbar}. \tag{37}$$

In order to proceed analytically with the integral in the numerator, we have to specify the T regime, as discussed in the next section.

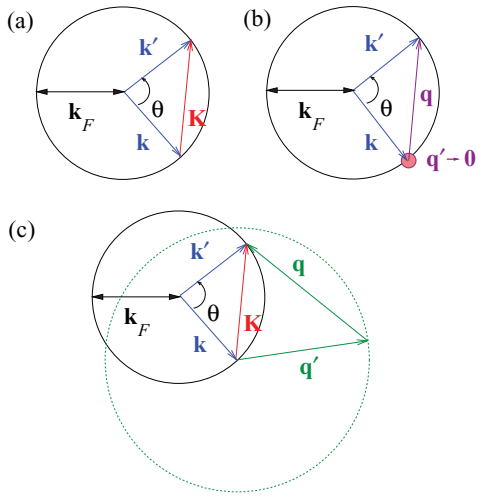

FIG. 1. (Color online) Scattering of electrons in momentum space due to (a) in-plane phonons, (b) nonstrained flexural, and (c) strained flexural phonons.

B. Bloch-Grüneisen temperature

For each scattering process (one- or two-phonon scattering), we may identify two different T regimes, *low* and *high* T, related to whether only small angle or every angle are available to scatter from $|\mathbf{k}\rangle$ to $|\mathbf{k}'\rangle$. Recall that since we are dealing with quasielastic scattering, both $\mathbf{k}$ and $\mathbf{k}'$ sit on the Fermi circle (see Fig. 1), and $|\mathbf{k}\rangle$ and $|\mathbf{k}'\rangle$ are adiabatically connected through a rotation of $\theta_{\mathbf{k},\mathbf{k}'}$ in momentum space. Large-angle scattering is only possible if phonons with high enough momentum are available to scatter electrons. The characteristic Bloch-Grüneisen (BG) temperature $T_{\rm BG}$ separating the two regimes may thus be set by the minimum phonon energy necessary to have full backscattering,

$$k_B T_{\rm BG} = \hbar\omega_{2k_F}, \tag{38}$$

with $\omega_{\mathbf{q}}$ as given in Sec. II.

For scattering by in-plane phonons, $T_{\rm BG}$ takes the value

$$T_{\rm BG}^{(L)} \approx 57\sqrt{n}\ {\rm K} \quad \text{and} \quad T_{\rm BG}^{(T)} \approx 38\sqrt{n}\ {\rm K} \tag{39}$$

for longitudinal and transverse phonons, respectively, with density n in units of 10^{12} cm^{-2}. When scattering is by two nonstrained FPs, the crossover between low- and high-T regimes is given by

$$T_{\rm BG} \approx 0.1n\ {\rm K}, \tag{40}$$

with n again measured in 10^{12} cm^{-2}, while in the presence of strain, using the approximated strained FP dispersion in Eq. (8), we get

$$T_{\rm BG} \simeq 28\sqrt{n\bar{u}}\ {\rm K}. \tag{41}$$

It is obvious from Eqs. (40) and (41) that the high-T regime is the relevant one for FP scattering.

C. Contributions to resistivity

In the following, we summarize our results for the T-dependent resistivity due to scattering by in-plane phonons and two FPs in bilayer graphene. For comparison, we discuss also the monolayer case first studied in Ref. 7. We use the variational method discussed in Sec. IV A, the resistivity being given by Eq. (36). Details on the derivation can be found in Appendix B. We neglect one FP processes since these, as can be seen in Eq. (23), are reduced by a factor $\sim h_0/L \ll 1$, where h_0 is the sample's vertical deflection over the typical linear size L.

1. Scattering by in-plane phonons

A sketch of the scattering process in momentum space involving one phonon is shown in Fig. 1(a). In this case, the resistivity can be written as (see Appendix B1)

$$\varrho_{in} \approx \frac{8\hbar k_F^2}{e^2\rho v_F^2 k_B T}\sum_\nu \int_0^1 dx\,\left[D_B^\nu(2x)\right]^2 \frac{x^4}{\sqrt{1-x^2}}\frac{e^{xz_\nu}}{(e^{xz_\nu}-1)^2}, \tag{42}$$

where $z_\nu = \hbar\omega_{2k_F}^\nu/k_B T$, with $\nu = L,T$, and where we have introduced a generalized electron–in-plane phonon coupling for bilayer graphene given by

$$D_B^\nu(y) = \left[2g^2y^2\left(1-\frac{y^2}{2}\right)^2\delta_{\nu L} + \frac{\hbar^2 v_F^2\beta^2}{4a^2}\left(1-\frac{y^2}{4}\right)\right]^{1/2}. \tag{43}$$

The case of scattering via screened scalar potential, here encoded in the screened deformation potential parameter g, has been considered recently in Ref. 32. As it is shown below, the gauge potential contribution becomes the dominant one in the low-T regime.

In the low-T regime $T \ll T_{\rm BG}$, we have $z_\nu \gg 1$, so that the integrand in Eq. (42) is only contributing significantly for $x \ll 1$. The generalized electron–in-plane phonon coupling in (43) then becomes

$$D_B^\nu(y \ll 1) = \left[2g^2y^2\delta_{\nu L} + \frac{\hbar^2 v_F^2\beta^2}{4a^2}\right]^{1/2}, \tag{44}$$

and the resistivity reads as

$$\varrho_{in} \approx \sum_\nu \left[g^2\frac{16\Gamma(6)\zeta(6)}{\Gamma(4)\zeta(4)}\left(\frac{T}{T_{\rm BG}}\right)^2\delta_{\nu L} + \frac{\hbar^2 v_F^2\beta^2}{4a^2}\right] \times \frac{\Gamma(4)\zeta(4)(k_B T)^4}{e^2\rho\hbar^4 v_F^2 v_\nu^5 k_F^3}, \tag{45}$$

where $\Gamma(n) = (n-1)!$ is the *gamma function* and $\zeta(n)$ is the *Riemann zeta function*. We have thus obtained the expected T^4 behavior at low T for coupling through gauge potential, which is the two-dimensional analog of the T^5 Bloch theory in three-dimensional metals.[29,33] The scalar potential contribution comes proportional to T^6 due to screening. It can be neglected in the low-T regime; even though $16\Gamma(6)\zeta(6)/[\Gamma(4)\zeta(4)] \approx 300$, it is strongly suppressed by $T/T_{\rm BG} \ll 1$ and $g < \hbar v_F\beta/(2a)$ (see Sec. III B).

In the high-T regime $T \gg T_{\rm BG}$, the inequality $z_\nu \ll 1$ holds, so that $e^{z_\nu x}/(e^{z_\nu x}-1)^2 \approx 1/(z_\nu x)$ in Eq. (42). The usual linearin T resistivity for one-phonon scattering is then recovered,

$$\varrho_{in} \approx \left(7g^2 + \frac{\hbar^2 v_F^2\beta^2}{8a^2}\frac{v_L^2}{\bar{v}^2}\right)\frac{\pi k_B T}{4\hbar\rho e^2 v_L^2 v_F^2}, \tag{46}$$

where $1/\bar{v}^2 = 1/v_L^2 + 1/v_T^2$. Note that, at odds with the low-T regime, now the scalar potential contribution is higher than that of the gauge potential for the typical coupling values discussed in Sec. III B.

The monolayer case has been discussed extensively in the literature.[6,7,18,33,34] The resistivity is still given by Eq. (42), only the generalized electron–in-plane phonon coupling changes:

$$D_M^{\nu}(y) = \left[2g^2y^2\left(1-\frac{y^2}{4}\right)\delta_{\nu L} + \frac{\hbar^2 v_F^2\beta^2}{4a^2}\right]^{1/2}. \quad (47)$$

The same qualitative behavior is obtained: At low T, the resistivity is given by Eq. (45) with the numerical replacement $16 \to 12$ in the scalar potential contribution; at high T, the result (46) holds with the replacement $(7g^2 + \frac{\hbar^2 v_F^2\beta^2}{8a^2}\frac{v_L^2}{\bar{v}^2}) \to (2g^2 + \frac{\hbar^2 v_F^2\beta^2}{2a^2}\frac{v_L^2}{\bar{v}^2})$. Note, however, the apparent quantitative difference: the scalar and gauge potential contributions change roles, the latter becoming more important in monolayer graphene. This is further discussed in Sec. V.

A final remark regarding the temperature-dependent resistivity due to in-plane phonons has to do with the value of the electron-phonon coupling parameters β and g. While β is expected to be restricted to the range $\beta \sim 2$–3, as discussed in Sec. III B, the value of the deformation potential parameter g is still debated in the literature. Phenomenology gives $g \sim$ 10–30 eV;[20,33] recent *ab initio* calculations provide a much smaller value $g \sim 3$ eV.[21] On the other hand, experiments seem to confirm the higher values, giving $g \sim$ 15–25 eV.[35,36] Our claim here is that all these values make sense, if properly interpreted. Phenomenology gives essentially unscreened deformation potential, which we called g_0 in Sec. III B, and which should take values of $\mathcal{O}(10)$ eV; screening effects suppress the deformation potential to $\mathcal{O}(1)$ eV, as we have seen in Sec. III B within the Thomas-Fermi approximation, in good agreement with *ab initio* results where screening is built in; the fact that transport experiments give a much higher deformation potential is a strong indication that phonon scattering through gauge potential, usually not included when fitting the data,[35,36] is at work. Indeed, by using the monolayer version of Eq. (46), we readily find that the fitting quantity in Refs. 35 and 36 should be replaced by

$$\tilde{D} = \left[2g^2 + \frac{v_F^2\hbar^2\beta^2}{2a^2}\left(1+\frac{v_L^2}{v_T^2}\right)\right]^{1/2}, \quad (48)$$

which, keeping $g \sim 3$ eV, takes values $\tilde{D} \sim$ 10–20 eV for $\beta \sim 2$–3, in excellent agreement with experiments. Moreover, since the gauge potential is not screened [Eq. (45)], it provides a natural explanation for the T^4 resistivity behavior recently reported at low T in Ref. 36, where the expected T^6 contribution due to scalar potential is absent.[32]

Typical T-dependent resistivity due to scattering by in-plane phonons [Eq. (42)] is shown in Fig. 2 as thick dashed lines. In agreement with analytical results, there is no qualitative difference between monolayer graphene [Fig. 2(a)] and bilayer graphene [Fig. 2(b)].

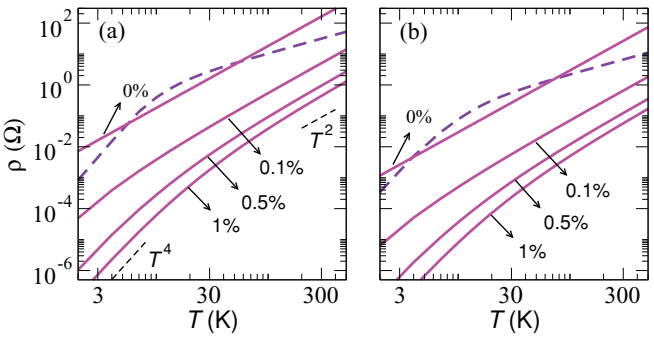

FIG. 2. (Color online) Resistivity vs T due to scattering by in-plane phonons (dashed thick lines) and flexural phonons (full lines) with and without strain (indicated in percentage) in (a) monolayer and (b) bilayer graphene. We use $n = 10^{12}$ cm^{-2}, $g \approx 3$ eV, and $\beta \approx 3$.

2. *Scattering by nonstrained flexural phonons*

In nonstrained bilayer graphene, scattering by FPs gives rise to the following T-dependent resistivity (details on the derivation are given in Appendix B2):

$$\varrho_F \approx \frac{\hbar k_F^2}{2\pi e^2\rho^2 v_F^2\alpha^2}\ln\left(\frac{k_B T}{\hbar\alpha q_c^2}\right) \times \int_0^1 dx \frac{\left[D_B^F(2x)\right]^2}{\sqrt{1-x^2}}\frac{x^4 e^{zx^2}}{(e^{zx^2}-1)^2}, \quad (49)$$

where $z = \hbar\omega_{2k_F}^F/k_B T$, and where the generalized electron-FP coupling for bilayer graphene is given by

$$D_B^F(x) = \left[g^2x^2\left(1-\frac{x^2}{2}\right)^2 + \frac{\hbar^2 v_F^2\beta^2}{4a^2}\left(1-\frac{x^2}{4}\right)\right]^{1/2}. \quad (50)$$

Equation (49) holds also for monolayer graphene, and we need only to introduce a different generalized electron-FP coupling

$$D_M(x) = \left[g^2x^2\left(1-\frac{x^2}{4}\right) + \frac{\hbar^2 v_F^2\beta^2}{4a^2}\right]^{1/2}. \quad (51)$$

In Fig. 1(b), a sketch of the two-phonon scattering process in momentum space is provided. It shows that one of the two phonons involved in the scattering event always has momentum $\mathbf{q}' \to 0$. This is a consequence of the quadratic FP dispersion [Eq. (4)], which leads to a divergent number of FPs with momentum $\mathbf{q}' \to 0$.[11] This divergence is responsible for the logarithmic factor in Eq. (49), which stems from the existence of an infrared cutoff q_c. This cutoff is to be identified with the onset of anharmonic effects,[38] or unavoidable built-in strain.[6]

In the low-T regime $T \ll T_{\rm BG}$, one has $z \gg 1$, so that the integrand in Eq. (49) is only contributing for $x \ll 1$. The generalized electron-phonon coupling becomes equal in both bilayer and monolayer systems,

$$D_B(y \ll 1) = D_M(y \ll 1) = \left[g^2y^2 + \frac{\hbar^2 v_F^2\beta^2}{4a^2}\right]^{1/2}, \quad (52)$$

and the resistivity is then the same in both:

$$\varrho_F \approx \left[g^2 \frac{6\Gamma(6)\zeta(6)}{\Gamma(4)\zeta(4)} \left(\frac{T}{T_{\rm BG}}\right)^2 + \frac{\hbar^2 v_F^2 \beta^2}{4a^2} \right] \frac{\Gamma(4)\zeta(4)\hbar k_F^2}{2^4 \pi e^2 \rho^2 v_F^2 \alpha^2} \times \left(\frac{k_B T}{\hbar \alpha k_F^2}\right)^{5/2} \ln\left(\frac{k_B T}{\hbar \alpha q_c^2}\right). \quad (53)$$

A similar result has been derived in Ref. 18. Owing to the same arguments used in the previous section for one-phonon scattering, we can neglect the scalar potential contribution at low T.

At high T, i.e., $T \gg T_{\rm BG}$, we have $z \ll 1$, so that $\exp(zx^2)/[\exp(zx^2)-1]^2 \approx 1/(zx^2)$ in Eq. (49). The bilayer graphene resistivity becomes

$$\varrho_F \approx \left(g^2 + \frac{\hbar^2 v_F^2 \beta^2}{8a^2}\right) \frac{(k_B T)^2}{64\hbar e^2 \rho^2 v_F^2 \alpha^4 k_F^2} \ln\left(\frac{k_B T}{\hbar \alpha q_c^2}\right). \quad (54)$$

This result holds for monolayer graphene with the substitution $(g^2 + \frac{\hbar^2 v_F^2 \beta^2}{8a^2}) \to (\frac{g^2}{2} + \frac{\hbar^2 v_F^2 \beta^2}{4a^2})$.[6,7] We have obtained that the resistivity due to nonstrained FPs is proportional to T^2/n, which implies mobility independent of the carrier density n. A similar result has been obtained in the context of microscopic ripples in graphene.[5,24] The result of Eq. (54) is shown in Fig. 2(b) as a full line indicating $\bar{u} \approx 0\%$. The logarithmic correction, expected to be of order unity in the relevant T range, has been ignored. Scattering by FPs dominates the contribution to resistivity in nonstrained samples at both low and high T, except for the crossover region where $T \sim T_{\rm BG}$ [Eq. (39)]. The same conclusion holds for monolayer graphene, the T dependent ϱ_F of which is shown in Fig. 2(a).

3. Scattering by strained flexural phonons

Applying strain breaks the membrane rotational symmetry inducing linear FP dispersion at low momentum, as can be seen in Eq. (8). A new energy scale appears in the problem,

$$\omega_{q^*}^F = \sqrt{2}\bar{u} v_L^2/\alpha \approx 10^4 \bar{u}\ {\rm K}, \quad (55)$$

separating two regimes: linear dispersion below and quadratic dispersion above. The associated momentum scale $q^* = \sqrt{\bar{u}} v_L/\alpha \approx 4.5\sqrt{\bar{u}}\ {\rm \AA}^{-1}$, together with k_F and the thermal momentum q_T given by $\hbar\omega_{q_T}^F = k_B T$, define all regimes where analytic treatment can be employed. In particular, in the low-T regime where $q_T \ll k_F$, we may always take $q^* \gg q_T$ and use a linear dispersion for FPs; otherwise, the nonstrained case considered in the previous section would be the appropriate starting point. In the high-T regime, we can distinguish between low strain for $q^* \ll q_T$ and high strain for $q^* \gg q_T$. Note that, at high T, relevant phonon scattering electrons have momentum q in the range $k_F \lesssim q \lesssim q_T$. Therefore, when strain is present in the high-T regime, we may always assume $q^* \gg k_F$; the opposite limit $q^* \ll k_F$ would again be identified with the nonstrained case considered previously.

The resistivity due to strained FPs can be cast in the form of a triple integral over rescaled momenta $x \to \tilde{x} = x\hbar v_L u^{1/2}/(k_B T)$ (see Appendix B2 for details):

$$\varrho_F \approx \frac{(k_B T)^6}{2^6 \pi^2 \hbar^5 e^2 \rho^2 v_F^2 v_L^8 \bar{u}^4 k_F^2} \times \int_0^{2\tilde{k}_F} d\tilde{K} \frac{\left[D_B^F(\tilde{K}/\tilde{k}_F)\right]^2 \tilde{K}^2}{\sqrt{\tilde{k}_F^2 - \tilde{K}^2/4}} \int_0^\infty d\tilde{q}\, \frac{\tilde{q}^3}{\omega_{\tilde{q}}} n_{\tilde{q}}(n_{\tilde{q}}+1) \times \int_{|\tilde{K}-\tilde{q}|}^{|\tilde{K}+\tilde{q}|} d\tilde{Q} \frac{\tilde{Q}^3 n_{\tilde{Q}}(n_{\tilde{Q}}+1)}{\omega_{\tilde{Q}} \sqrt{\tilde{q}^2\tilde{K}^2 - (\tilde{K}^2+\tilde{q}^2-\tilde{Q}^2)^2/4}} \times \left(\frac{\omega_{\tilde{q}}+\omega_{\tilde{Q}}}{1+n_{\tilde{q}}+n_{\tilde{Q}}} - \frac{\omega_{\tilde{q}}-\omega_{\tilde{Q}}}{n_{\tilde{q}}-n_{\tilde{Q}}}\right), \quad (56)$$

where the rescaled dispersion reads as $\omega_{\tilde{x}} \approx \sqrt{\gamma^2\tilde{x}^4 + \tilde{x}^2}$, with $\gamma = \sqrt{2}\omega_{q_T}^F/\omega_{q^*}^F$, and the generalized electron-FP coupling $D_B^F(y)$ is given by Eq. (50). For monolayer graphene, only the coupling changes, being given instead by Eq. (51). The kinematics of the scattering process is schematically shown in Fig. 1(c).

In the low-T case $T \ll T_{\rm BG}$, we have only small-angle scattering with $K \ll k_F$. The argument of the generalized electron-FP coupling becomes small $K/k_F \ll 1$, and it can be written as

$$D_B(y \ll 1) \approx D_M(y \ll 1) \approx \left[g^2 y^2 + \frac{\hbar^2 v_F^2 \beta^2}{4a^2}\right]^{1/2}. \quad (57)$$

The resistivity is the same in both bilayer and monolayer systems. Since the inequality $q_T \ll k_F, q^*$ holds, relevant phonons have linear dispersion $\omega_q^F \approx \sqrt{\bar{u}} v_L q$ and the rescaled Fermi momentum obeys $\tilde{k}_F \approx k_F/q_T \gg 1$. We may take $\tilde{K} \to \infty$ as the upper limit in the $\tilde{K}$ integral in Eq. (56), and the resistivity is then approximated by

$$\varrho_F \approx \left[g^2 \left(\frac{q_T}{k_F}\right)^2 \mathcal{K}_4 + \frac{\hbar^2 v_F^2 \beta^2}{4a^2} \mathcal{K}_2 \right] \times \frac{(k_B T)^7}{2^6 \pi^2 \hbar^6 e^2 \rho^2 v_F^2 v_L^9 \bar{u}^{9/2} k_F^3}, \quad (58)$$

where

$$\mathcal{K}_n = \int_0^\infty d\tilde{K} \tilde{K}^n \int_0^\infty d\tilde{q}\, q^2 n_{\tilde{q}}(n_{\tilde{q}}+1) \times \int_{|\tilde{K}-\tilde{q}|}^{|\tilde{K}+\tilde{q}|} d\tilde{Q} \frac{\tilde{Q}^2 n_{\tilde{Q}}(n_{\tilde{Q}}+1)\left(\frac{\tilde{q}+\tilde{Q}}{1+n_{\tilde{q}}+n_{\tilde{Q}}} - \frac{\tilde{q}-\tilde{Q}}{n_{\tilde{q}}-n_{\tilde{Q}}}\right)}{\sqrt{\tilde{q}^2\tilde{K}^2 - (\tilde{K}^2+\tilde{q}^2-\tilde{Q}^2)^2/4}}. \quad (59)$$

It can be shown numerically that $\mathcal{K}_2 \approx 4485$ and $\mathcal{K}_4 \approx 496\,850$. The large ratio $\mathcal{K}_4/\mathcal{K}_2 \gg 1$ is, however, compensated by $q_T/k_F \ll 1$ and the fact that $g < \hbar v_F \beta/(2a)$ (see Sec. III B). As in the case of scattering by in-plane phonons, also here the gauge potential contribution to resistivity dominates at low T.

Now we consider the high-T regime $T \gg T_{BG}$. At odds with the nonstrained case [see Fig. 1(b)], now phonons with momentum q in the range $k_F \lesssim q \lesssim q_T$ provide most of the scattering. It is shown in Appendix B2b that the integral over

$\tilde{Q}$ in Eq. (56) becomes $\tilde{K}$ independent, and the $\tilde{q}$ integral can be cast in the form

$$\mathcal{G}(\gamma) = \int_0^\infty d\tilde{q}\, \frac{\tilde{q}^5 n_{\tilde{q}}^2 (n_{\tilde{q}}+1)^2}{\gamma^2\tilde{q}^4+\tilde{q}^2} \times \left(\frac{2\sqrt{\gamma^2\tilde{q}^4+\tilde{q}^2}}{1+2n_{\tilde{q}}} + \frac{1}{n_{\tilde{q}}(n_{\tilde{q}}+1)} \right), \quad (60)$$

being easily evaluated numerically. The resistivity in bilayer graphene can then be written as

$$\varrho_F \approx \left(7g^2 + \frac{\hbar^2 v_F^2 \beta^2}{4a^2}\right) \frac{(k_B T)^4}{2^7 \hbar^3 e^2 \rho^2 v_F^2 v_L^6 \bar{u}^3} \mathcal{G}\left(\frac{\alpha k_B T}{\hbar \bar{u} v_L^2}\right). \quad (61)$$

When $\gamma \ll 1$, or equivalently $q_T \ll q^*$ (high strain), the function $\mathcal{G}(\gamma)$ behaves as $\mathcal{G}(\gamma \ll 1) \approx 18\zeta(3) - 93\zeta(5)/8$. For $\gamma \gg 1$, or equivalently $q_T \gg q^*$ (small strain), it gives $\mathcal{G}(\gamma \gg 1) \approx 1/\gamma^2$. In these asymptotic regimes, one can obtain analytic expressions for the resistivity in Eq. (61):

$$\varrho_F \approx \left(7g^2 + \frac{\hbar^2 v_F^2 \beta^2}{4a^2}\right) \frac{1}{2^7 \hbar^3 e^2 v_F^2} \times \begin{cases} \left[18\zeta(3) - \frac{93}{8}\zeta(5)\right] \frac{(k_B T)^4}{\rho^2 v_L^6 \bar{u}^3} & k_F \ll q_T \ll q^*, \\ \frac{\hbar^2 (k_B T)^2}{\rho \kappa v_L^2 \bar{u}} & k_F \ll q^* \ll q_T. \end{cases} \quad (62)$$

Equations (61) and (62) also hold for monolayer graphene with $(7g^2 + \frac{\hbar^2 v_F^2 \beta^2}{4a^2}) \to (2g^2 + \frac{\hbar^2 v_F^2 \beta^2}{a^2})$.

The effect of strain in the T dependence of resistivity is shown in Fig. 2(a) for monolayer graphene and in Fig. 2(b) for bilayer at strain values $\bar{u} \approx 0.1\%$, 0.5%, and 1%. The crossover between the two regimes of Eq. (61) [see Eq. (62)] is clearly seen at $\gamma \approx 1$, which is equivalent to $T \approx 10^4 \bar{u}$ K. It is apparent from Fig. 2 that the contribution to the resistivity due to scattering by FPs is strongly suppressed by applying strain.

D. Crossover between in-plane- and flexural-phonon dominated scattering

Scattering by in-plane and flexural phonons is always at work simultaneously. However, the two mechanisms provide completely different T-dependent resistivity, and therefore we expect them to dominate at different T. In the following, we address the transition T at which $\varrho_{in} \approx \varrho_F$.

1. Nonstrained case

In this case, using Eqs. (46) and (54) for bilayer graphene in the high-T regime, we get

$$\frac{\varrho_F}{\varrho_{in}} \approx \frac{T[K]}{75n\ [\mathrm{cm}^{-2}]}. \quad (63)$$

We expect a crossover between in-plane to FP dominated scattering given by

$$T_{c2} \approx 75n\ [\mathrm{cm}^{-2}]\ \mathrm{K}. \quad (64)$$

The T_c just obtained is close to T_{BG} for in-plane phonons [Eq. (39)] and much higher than T_{BG} for FPs [Eq. (40)]. By using the low-T approximation for ϱ_{in} [Eq. (45)], we obtain the ratio

$$\frac{\varrho_F}{\varrho_{in}} \approx 12 \frac{\sqrt{n\ [\mathrm{cm}^{-2}]}}{(T\ [\mathrm{K}])^2}, \quad (65)$$

from which we expect a crossover from FP to in-plane dominated scattering at

$$T_{c1} \approx 3(n\ [\mathrm{cm}^{-2}])^{1/4}\ \mathrm{K} \quad (66)$$

as T increases. We conclude that scattering by FP always dominates over scattering by in-plane phonons, except for the region $T_{c1} \ll T \ll T_{c2}$ around T_{BG} for in-plane phonons [Eq. (39)]. This is clearly seen in Fig. 2(b). The same conclusion applies to monolayer graphene. In this latter case, we obtain $T_{c1} \approx 6(n\ [\mathrm{cm}^{-2}])^{1/4}$ K and $T_{c2} \approx 55n\ [\mathrm{cm}^{-2}]$ K.

2. Strained case

It can easily be shown that the crossover from in-plane to flexural phonon dominated scattering always occurs in the low-strain regime $q^* \ll q_T$. We have seen in the previous sections that the crossover temperature T separating high-strain from low-strain behavior is given by $\gamma = \sqrt{2}\omega_{q_T}^F / \omega_{q^*}^F \approx 1$. By using Eq. (55), we get a crossover temperature $T^* \approx 10^4 \bar{u}$ K. On the other hand, by using the low-strain approximation for the resistivity due to flexural phonons given in Eq. (62) and the resistivity due to in-plane phonons in Eq. (46), we obtain for the ratio in bilayer graphene

$$\frac{\varrho_F}{\varrho_{in}} \approx \frac{k_B T}{40\pi\kappa\bar{u}}. \quad (67)$$

The corresponding crossover T then reads as

$$T_c \approx 10^6 \bar{u}\ \mathrm{K}. \quad (68)$$

Clearly, $T_c \gg T^*$, justifying our low-strain approximation. The same applies to monolayer graphene under strain. The resistivity ratio is in that case $\varrho_F/\varrho_{in} \approx k_B T/(50\pi\kappa\bar{u})$, from which we obtain roughly the same T_c even taking into account that κ in monolayer is half that of bilayer in our elasticity model.

An important conclusion may be drawn. While in the nonstrained case scattering by FP is the dominant contribution to the resistivity, it can be seen from Eq. (68) that applying small amounts of strain is enough to suppress this contribution at room temperature. This is clearly seen in Fig. 2.

V. DISCUSSION

We have found the T-dependent resistivity due to acoustic phonons to be qualitatively similar in monolayer and bilayer graphene (see Sec. IV C). This becomes apparent when we compare Figs. 2(a) and 2(b) where $\varrho(T)$ is shown, respectively, for monolayer and bilayer graphene both at zero and finite strain. Such behavior can be traced back to the resistivity expression [Eq. (36)], or more precisely to its numerator, where the different electronic structure and electron-phonon coupling conspire to give exactly the same parametric dependence in monolayer and bilayer graphene. In short, it can be readily seen through Eq. (36) that the information about the electronic structure enters via the density of states squared

in the numerator. The electron-phonon coupling, in its turn, enters through the transition rate $\mathcal{P}_{\mathbf{k},\mathbf{k}'}$, and in the Born approximation it also appears squared. When coupling is via scalar potential [V_1 matrix elements in Eq. (23)], the screening makes the coupling inversely proportional to the density of states, and the square of it cancels exactly with the square density of states coming from the integral over $\mathbf{k}$ and $\mathbf{k}'$ in the numerator of Eq. (36). For the coupling through gauge potential [V_2 matrix elements in Eq. (23)], the parametric difference between monolayer and bilayer amounts to the replacement $v_F^2 \to \hbar^2 k_F^2/(2m)^2$ (after taking the square of the matrix elements and using the quasielastic approximation). When multiplied by the square of the density of states in bilayer graphene $\mathcal{D}(E) \sim m/\hbar^2$, we obtain the factor $k_F^2/\hbar^2$, which has exactly the same parametric dependence appearing for single-layer graphene; there, the factor v_F^2 multiplies the square of the density of states of the monolayer, $\mathcal{D}(E) \sim k/(\hbar v_F)$.

Despite qualitative similarities, there are apparent quantitative differences. A striking one is the overall suppression of resistivity in bilayer graphene, which is clearly seen when we compare Figs. 2(a) and 2(b). This is due to the higher stiffness and mass density of bilayer graphene (see Sec. II), and to the $1/2$ term in Eq. (17) for the gauge potential which, at odds with the parametric dependence just discussed, does not cancel out in the expression for the resistivity. Also, the scalar potential contribution is quantitatively different, being enhanced in bilayer graphene, as can be seen by comparing Eqs. (45) and (46), Eqs. (53) and (54), and Eqs. (58) and (61) with their monolayer counterparts. This arises because pseudospin conservation allows backscattering due to scalar potential in bilayer but not in monolayer graphene.

The quantitative discrepancy between the T-dependent resistivity in bilayer and monolayer graphene originates an interesting difference regarding room-temperature mobility in nonstrained samples. The mobility μ, defined as $\varrho = 1/(en\mu)$, is in the nonstrained case limited by PF scattering (see Sec. IV C 2) and takes the form

$$\mu \approx \mathcal{A}\frac{64\pi\hbar e v_F^2}{k_B^2 T^2}, \tag{69}$$

with $\mathcal{A}_B = \kappa^2/[g^2 + \hbar^2 v_F^2 \beta^2/(8a^2)]$ in bilayer graphene and $\mathcal{A}_M = \kappa^2/[g^2/2 + \hbar^2 v_F^2 \beta^2/(4a^2)]$ in monolayer graphene, ignoring the logarithmic contribution of order unity [Eq. (54)]. For monolayer graphene at room temperature, the mobility is limited to the value for samples on substrate, $\mu \approx 198\mathcal{A}_M \sim 1$ m^2/Vs, as has recently been confirmed experimentally.[6] For bilayer graphene, however, the quantitative differences discussed above lead to an enhanced room-temperature mobility $\mu \approx 198\mathcal{A}_B \sim 20$ m^2/Vs. This might be an interesting aspect to take into account regarding room-temperature electronic applications. Reports of much smaller mobility (one order of magnitude) in recent experiments in suspended bilayer graphene[1] might be an indication that residual,[37] presumably T-independent, scattering is at work, overcoming the intrinsic FP contribution.

Another remark worthy of discussion is the validity of results in the nonstrained regime, in particular Eq. (54), for the high-T resistivity. At low densities, when k_F becomes comparable with the infrared cutoff q_c given by the onset of anharmonic effects,[38] the harmonic approximation used here breaks down. A complete theory would require taking into account anharmonicities, but this is beyond the scope of this paper. Nevertheless, it is likely that unavoidable little strain u is always present in real samples,[6] and this increases the validity of the harmonic approximation.[39] Moreover, the infrared cutoff q_c due to anharmonic effects depends on the applied strain (see supplementary material[40]), decreasing as strain increases. This is consistent with sample-to-sample mobility differences of order unity recently reported in suspended monolayer graphene,[6] where strain $u \lesssim 10^{-4}$–10^{-3} is naturally expected.

Finally, we comment on a recent theory paper by Mariani and von Oppen[7] where the T-dependent resistivity of monolayer graphene has been fully discussed. In the high-T regime $T \gg T_{\mathrm{BG}}$, our results for the monolayer case agree with those of Ref. 7. However, at low T, i.e. $T \ll T_{\mathrm{BG}}$, the authors of Ref. 7 found a new regime where the scalar potential contribution dominates. This happens because, in Ref. 7, the electron-phonon coupling from scalar potential is assumed to be much higher than the gauge potential coupling, unless $T \ll T_{\mathrm{GD}}$, where T_{GD} is the energy scale at which screening becomes relevant and scalar and gauge potentials become comparable. The new regime arises for $T_{\mathrm{GD}} \ll T \ll T_{\mathrm{BG}}$. With the parameter values used in this paper, however, the electron-phonon coupling due to scalar potential is always similar or smaller than the gauge potential (see Sec. III B). Therefore, we can neglect this low-T contribution since it gives higher power-law behavior than the gauge potential. Recent T-dependent resistivity due to in-plane phonons measured in single-layer graphene at the high densities[36] seems to corroborate the latter picture.

VI. CONCLUSIONS

In this paper, we have studied the T-dependent resistivity due to scattering by both acoustic in-plane phonons and FPs in doped, suspended bilayer graphene. We have found the bilayer membrane to follow the qualitative behavior of the monolayer cousin.[6,7] Different electronic structure combine with different electron-phonon coupling to give the same parametric dependence in resistivity and, in particular, the same T behavior. In parallel with the single layer, FPs dominate the phonon contribution to resistivity in the absence of strain, where a density-independent mobility is obtained. This contribution is strongly suppressed by tension, similar to monolayer graphene.[6] However, an interesting quantitative difference with respect to suspended monolayer graphene has been found. In the latter, as shown in Ref. 6, FPs limit room-temperature mobility μ to values obtained for samples on substrate $\mu \sim 1$ m^2/(Vs) when tension is absent. In bilayer graphene, quantitative differences in electron-phonon coupling and elastic constants lead to a room-temperature mobility enhanced by one order of magnitude $\mu \sim 20$ m^2/(Vs), even in nonstrained samples. This finding has obvious advantages for room-temperature electronic applications. It has also been shown that, for a correct description of acoustic phonon scattering in both monolayer and bilayer graphene, even at the qualitative level, coupling to both scalar and gauge potentials needs to be taken into account.

ACKNOWLEDGMENTS

We acknowledge financial support from MICINN (Spain) through Grant No. FIS2008-00124 and from CONSOLIDER Grant No. CSD2007-00010, and from the Comunidad de Madrid, through NANOBIOMAG. H.O. acknowledges financial support through grants from JAE-Pre (CSIC, Spain). E.V.C. acknowledges financial support from the Juan de la Cierva Program (MICINN, Spain) and the Program "Estímulo à Investigação" of Gulbenkian Foundation, Portugal. M.I.K. acknowledges financial support from FOM (The Netherlands).

APPENDIX A: COLLISION INTEGRAL

The rate of change of $f_{\mathbf{k}}$ due to scattering, the so-called collision integral $\dot{f}_{\mathbf{k}}|_{\rm scatt}$ appearing on the right-hand side of the Boltzmann equation (24), is the difference between the rate at which quasiparticles enter the state $|\mathbf{k}\rangle$ and the rate at which they leave it:

$$\dot{f}_{\mathbf{k}}|_{\rm scatt} = \sum_{\mathbf{k}'} \left[f_{\mathbf{k}'}(1-f_{\mathbf{k}})\mathcal{W}_{\mathbf{k}'}^{\mathbf{k}} - f_{\mathbf{k}}(1-f_{\mathbf{k}'})\mathcal{W}_{\mathbf{k}}^{\mathbf{k}'} \right], \quad \text{(A1)}$$

where $\mathcal{W}_i^f$ is the scattering probability between states $|i\rangle$ and $|f\rangle$. Here, we use Fermi's golden rule, which reads as

$$\mathcal{W}_i^f = \frac{2\pi}{\hbar} |\langle f|\mathcal{H}_{\rm int}|i\rangle|^2 \delta(\mathcal{E}_f - \mathcal{E}_i), \quad \text{(A2)}$$

and is equivalent to rest upon the Born approximation for the differential scattering cross section.

The crucial step to get $\dot{f}_{\mathbf{k}}|_{\rm scatt}$ is finding the scattering probability for a quasiparticle in state $|\mathbf{k}\rangle$ to be scattered into state $|\mathbf{k}'\rangle$, i.e., $\mathcal{W}_{\mathbf{k}}^{\mathbf{k}'}$ (since the process is quasielastic, interband transitions are not allowed). The scattering mechanism is encoded in the interaction $\mathcal{H}_{\rm int}$, which, in the present case, is given by $H_{e\text{-}p}$ in Eq. (22). It is readily seen that scattering occurs only through emission or absorption of one phonon or emission or absorption of two phonons. The initial and final states are thus tensorial products of the form $|i\rangle = |\mathbf{k}\rangle \otimes |n_{\mathbf{q}}\rangle$ or $|i\rangle = |\mathbf{k}\rangle \otimes |n_{\mathbf{q}}, n_{\mathbf{q}'}\rangle$, and $|f\rangle = |\mathbf{k}'\rangle \otimes |n_{\mathbf{q}} \pm 1\rangle$, $|f\rangle = |\mathbf{k}'\rangle \otimes |n_{\mathbf{q}} \pm 1, n_{\mathbf{q}'} \pm 1\rangle$ or $|f\rangle = |\mathbf{k}'\rangle \otimes |n_{\mathbf{q}} \pm 1, n_{\mathbf{q}'}^F \mp 1\rangle$, where $|n_{\mathbf{q}}\rangle$ and $|n_{\mathbf{q}}, n_{\mathbf{q}'}\rangle$ represent one- and two-phonon states in the occupation number representation,[18] and the electronlike quasiparticle state is written according to the unitary transformation in Eq. (10) as $|\mathbf{k}\rangle = (e^{-i\theta_{\mathbf{k}}} a_{\mathbf{k}}^\dagger |0\rangle + e^{i\theta_{\mathbf{k}}} b_{\mathbf{k}}^\dagger |0\rangle)/\sqrt{2}$ (electron-hole symmetry guarantees the result is the same for both electron and hole doping).

In order to obtain $|\langle f|H_{e\text{-}p}|i\rangle|^2$, with $|i\rangle$ and $|f\rangle$ as given above, we take the following steps. (i) Terms of the form $V_1 V_2$, where V_1 stands for scalar potential and V_2 for gauge potential induced matrix elements in Eq. (23), are neglected. It is easy to show that such terms come proportional to oscillatory factors $e^{\pm i2\theta_{\mathbf{k}}}$ or $e^{\pm i2\theta_{\mathbf{k}'}}$ (in monolayer graphene $e^{\pm i\theta_{\mathbf{k}}}$ or $e^{\pm i\theta_{\mathbf{k}'}}$), stemming from the unitary transformation in Eq. (10). These terms can safely be neglected in doing the summation over the direction of $\mathbf{k}$ and $\mathbf{k}'$ in the numerator of Eq. (36), keeping $\theta_{\mathbf{k},\mathbf{k}'}$ fixed. The resistivity is then the sum of two independent contributions, originating from scalar and gauge potentials, well in the spirit of Matthiessen's empirical rule.[29] (ii) The scalar potential contribution is proportional to the overlap of states belonging to the same band

$$\left| V_{1,\mathbf{q}}^v \frac{e^{i(\theta_{\mathbf{k}'}-\theta_{\mathbf{k}})}}{2} + V_{1,\mathbf{q}}^v \frac{e^{-i(\theta_{\mathbf{k}'}-\theta_{\mathbf{k}})}}{2} \right|^2 = \left| V_{1,\mathbf{q}}^v \right|^2 \frac{1+\cos 2\theta_{\mathbf{k},\mathbf{k}'}}{2}. \quad \text{(A3)}$$

The same manipulation holds for two-phonon terms, with $V_{1,\mathbf{q}}^v \to V_{1,\mathbf{q},\mathbf{q}'}^F$. (iii) For the gauge potential contribution, there are oscillatory terms that, owing to the argument of point (i), can be neglected:

$$\left| V_{2,\mathbf{q},\mathbf{k},\mathbf{k}'}^v \frac{e^{i(\theta_{\mathbf{k}'}+\theta_{\mathbf{k}})}}{2} + \left(V_{2,-\mathbf{q},\mathbf{k},\mathbf{k}'}^v\right)^* \frac{e^{-i(\theta_{\mathbf{k}'}+\theta_{\mathbf{k}})}}{2} \right|^2 \simeq \left| \tilde{V}_{2,\mathbf{q}}^v \right|^2 \left(\frac{k^2}{2} + \frac{k'^2}{2} + kk' \cos\theta_{\mathbf{k},\mathbf{k}'} \right), \quad \text{(A4)}$$

where we used $\tilde{V}$ to express the matrix elements given in Eq. (23) for bilayer graphene without the term $(\pi_{\mathbf{k}} + \pi_{\mathbf{k}'})$. A similar manipulation holds for two-phonon terms, with $\tilde{V}_{2,\mathbf{q}}^v \to \tilde{V}_{2,\mathbf{q},\mathbf{q}'}^F$.

Finally, by summing over phonon momenta and doing the thermal average, we can write $\mathcal{W}_{\mathbf{k}}^{\mathbf{k}'}$ as follows: When scattering is via one phonon,

$$\mathcal{W}_{\mathbf{k}}^{\mathbf{k}'} = \frac{\pi}{\hbar} \sum_{\mathbf{q}} w_v(\mathbf{q},\mathbf{k},\mathbf{k}') n_{\mathbf{q}} \delta_{\mathbf{k}',\mathbf{k}+\mathbf{q}} \delta\left(\varepsilon_{\mathbf{k}'} - \varepsilon_{\mathbf{k}} - \hbar\omega_{\mathbf{q}}^v\right) + \frac{\pi}{\hbar} \sum_{\mathbf{q}} w_v(\mathbf{q},\mathbf{k},\mathbf{k}')(n_{\mathbf{q}}+1) \delta_{\mathbf{k}',\mathbf{k}-\mathbf{q}} \delta\left(\varepsilon_{\mathbf{k}'} - \varepsilon_{\mathbf{k}} + \hbar\omega_{\mathbf{q}}^v\right), \quad \text{(A5)}$$

where the first term is due to absorption and the second to emission of a single phonon; when scattering involves two phonons,

$$\begin{aligned} \mathcal{W}_{\mathbf{k}}^{\mathbf{k}'} = {} & \frac{\pi}{\hbar} \sum_{\mathbf{q},\mathbf{q}'} w_F(\mathbf{q},\mathbf{q}',\mathbf{k},\mathbf{k}') n_{\mathbf{q}} n_{\mathbf{q}'} \\ & \times \delta_{\mathbf{k}',\mathbf{k}+\mathbf{q}+\mathbf{q}'} \delta\left(\varepsilon_{\mathbf{k}'} - \varepsilon_{\mathbf{k}} - \hbar\omega_{\mathbf{q}}^F - \hbar\omega_{\mathbf{q}'}^F\right) \\ & + \frac{\pi}{\hbar} \sum_{\mathbf{q},\mathbf{q}'} w_F(\mathbf{q},\mathbf{q}',\mathbf{k},\mathbf{k}')(n_{\mathbf{q}}+1)(n_{\mathbf{q}'}+1) \\ & \times \delta_{\mathbf{k}',\mathbf{k}-\mathbf{q}-\mathbf{q}'} \delta\left(\epsilon_{\mathbf{k}'} - \epsilon_{\mathbf{k}} + \hbar\omega_{\mathbf{q}}^F + \hbar\omega_{\mathbf{q}'}^F\right) \\ & + \frac{2\pi}{\hbar} \sum_{\mathbf{q},\mathbf{q}'} w_F(\mathbf{q},\mathbf{q}',\mathbf{k},\mathbf{k}')(n_{\mathbf{q}}+1) n_{\mathbf{q}'} \\ & \times \delta_{\mathbf{k}',\mathbf{k}-\mathbf{q}+\mathbf{q}'} \delta\left(\epsilon_{\mathbf{k}'} - \epsilon_{\mathbf{k}} + \hbar\omega_{\mathbf{q}}^F - \hbar\omega_{\mathbf{q}'}^F\right), \end{aligned} \quad \text{(A6)}$$

where the first term is due to absorption of two FPs, the second to emission of two FPs, and the last one comes from absorption of a single FP and emission of another one. The kernels $w_v(\mathbf{q},\mathbf{k},\mathbf{k}')$ and $w_F(\mathbf{q},\mathbf{q}',\mathbf{k},\mathbf{k}')$ represent the sum of the right-hand side of Eq. (A3) with (A4), as given in Eq. (34). For monolayer graphene, $\mathcal{W}_{\mathbf{k}}^{\mathbf{k}'}$ take exactly the same form;[7] only the kernels change, being given instead by Eq. (35). The collision integral may finally be put in the form

$$\begin{aligned} \dot{f}_{\mathbf{k}}|_{\rm scatt} = {} & \frac{\pi}{\hbar} \sum_{\mathbf{k}'} \sum_{\mathbf{q},v} w_v(\mathbf{q},\mathbf{k},\mathbf{k}') \\ & \times \{[f_{\mathbf{k}'}(1-f_{\mathbf{k}}) n_{\mathbf{q}} - f_{\mathbf{k}}(1-f_{\mathbf{k}'})(n_{\mathbf{q}}+1)] \\ & \times \delta_{\mathbf{k},\mathbf{k}'+\mathbf{q}} \delta(\varepsilon_{\mathbf{k}} - \varepsilon_{\mathbf{k}'} - \hbar\omega_{\mathbf{q}}^v) \end{aligned}$$

$$+\left[f_{\mathbf{k}'}(1-f_{\mathbf{k}})(n_{\mathbf{q}}+1)-f_{\mathbf{k}}(1-f_{\mathbf{k}'})n_{\mathbf{q}}\right]\times\delta_{\mathbf{k},\mathbf{k}'-\mathbf{q}}\delta(\varepsilon_{\mathbf{k}}-\varepsilon_{\mathbf{k}'}+\hbar\omega_{\mathbf{q}}^{\nu})\}\tag{A7}$$

for one-phonon scattering processes, and

$$\begin{aligned}\dot{f}_{\mathbf{k}}\big|_{\text{scatt}} &= \frac{\pi}{\hbar}\sum_{\mathbf{k}'}\sum_{\mathbf{q},\mathbf{q}'} w_F(\mathbf{q},\mathbf{q}',\mathbf{k},\mathbf{k}')\\ &\times\{[f_{\mathbf{k}'}(1-f_{\mathbf{k}})(n_{\mathbf{q}}+1)(n_{\mathbf{q}'}+1)-f_{\mathbf{k}}(1-f_{\mathbf{k}'})n_{\mathbf{q}}n_{\mathbf{q}'}]\\ &\times\delta_{\mathbf{k},\mathbf{k}'-\mathbf{q}-\mathbf{q}'}\delta\left(\varepsilon_{\mathbf{k}}-\varepsilon_{\mathbf{k}'}+\hbar\omega_{\mathbf{q}}^{F}+\hbar\omega_{\mathbf{q}'}^{F}\right)\\ &+[f_{\mathbf{k}'}(1-f_{\mathbf{k}})(n_{\mathbf{q}}+1)n_{\mathbf{q}'}-f_{\mathbf{k}}(1-f_{\mathbf{k}'})n_{\mathbf{q}}(n_{\mathbf{q}'}+1)]\\ &\times\delta_{\mathbf{k},\mathbf{k}'-\mathbf{q}+\mathbf{q}'}\delta\left(\varepsilon_{\mathbf{k}}-\varepsilon_{\mathbf{k}'}+\hbar\omega_{\mathbf{q}}^{F}-\hbar\omega_{\mathbf{q}'}^{F}\right)\\ &+[f_{\mathbf{k}'}(1-f_{\mathbf{k}})n_{\mathbf{q}}n_{\mathbf{q}'}-f_{\mathbf{k}}(1-f_{\mathbf{k}'})(n_{\mathbf{q}}+1)(n_{\mathbf{q}'}+1)]\\ &\times\delta_{\mathbf{k},\mathbf{k}'+\mathbf{q}+\mathbf{q}'}\delta(\varepsilon_{\mathbf{k}}-\varepsilon_{\mathbf{k}'}-\hbar\omega_{\mathbf{q}}^{F}-\hbar\omega_{\mathbf{q}'}^{F})\\ &+[f_{\mathbf{k}'}(1-f_{\mathbf{k}})n_{\mathbf{q}}(n_{\mathbf{q}'}+1)-f_{\mathbf{k}}(1-f_{\mathbf{k}'})(n_{\mathbf{q}}+1)n_{\mathbf{q}'}]\\ &\times\ \delta_{\mathbf{k},\mathbf{k}'+\mathbf{q}-\mathbf{q}'}\delta\left(\varepsilon_{\mathbf{k}}-\varepsilon_{\mathbf{k}'}-\hbar\omega_{\mathbf{q}}^{F}+\hbar\omega_{\mathbf{q}'}^{F}\right)\}\end{aligned}\tag{A8}$$

for scattering through two FPs.

Now, we derive the linearized version of the collision integrals given in Eqs. (A7) and (A8). We start by expanding electron and phonon probability distributions around their equilibrium values

$$f_{\mathbf{k}}=f_{\mathbf{k}}^{(0)}+\delta f_{\mathbf{k}},\qquad n_{\mathbf{q}}=n_{\mathbf{q}}^{(0)}+\delta n_{\mathbf{q}},\tag{A9}$$

where the variations can be written as $\delta f_{\mathbf{k}}=-\frac{\partial f_{\mathbf{k}}^{(0)}}{\partial\varepsilon_{\mathbf{k}}}\varphi_{\mathbf{k}}$ [see Eq. (26)] and $\delta n_{\mathbf{q}}=-\frac{\partial n_{\mathbf{q}}^{(0)}}{\partial(\hbar\omega_{\mathbf{q}})}\chi_{\mathbf{q}}$. The linearized collision integral $\delta\dot{f}_{\mathbf{k}}|_{\text{scatt}}$ is then obtained by expanding $\dot{f}_{\mathbf{k}}|_{\text{scatt}}$ up to first order in the variations.[29,41]

The one-phonon scattering case follows closely the steps outlined in Ref. 41 and, for the case of monolayer graphene, it has been derived in Ref. 7. Since the difference between monolayer and bilayer amounts to a different kernel $w_{\nu}(\mathbf{q},\mathbf{k},\mathbf{k}')$ in Eqs. (A7), which does not play any role in the linearization, we can directly apply the result of Ref. 7 to the present case. In order to set notation for the more elaborated case of two-phonon scattering, we outline the main steps of the derivation in the following. We first note that, at equilibrium, detailed balance implies $\dot{f}_{\mathbf{k}}^{(0)}|_{\text{scatt}}=0$, from which we get the relation

$$f_{\mathbf{k}'}^{(0)}\left(1-f_{\mathbf{k}}^{(0)}\right)n_{\mathbf{q}}^{(0)}=f_{\mathbf{k}}^{(0)}\left(1-f_{\mathbf{k}'}^{(0)}\right)\left(n_{\mathbf{q}}^{(0)}+1\right),\tag{A10}$$

which can be easily verified by direct calculation.[41] Therefore, in order to get the linearized collision integral, it is enough to calculate the variation

$$\delta[f_{\mathbf{k}'}(1-f_{\mathbf{k}})n_{\mathbf{q}}-f_{\mathbf{k}}(1-f_{\mathbf{k}'})(n_{\mathbf{q}}+1)].\tag{A11}$$

A straightforward calculation (see supplementary material for details[40]) allows us to write this variation in terms of the equilibrium distributions and $\varphi_{\mathbf{k}}$, $\chi_{\mathbf{q}}$. Then, we introduce two typical approximations: We consider phonons at equilibrium by taking $\chi_{\mathbf{q}}\approx 0$, so that $n_{\mathbf{q}}\approx n_{\mathbf{q}}^{(0)}$, valid at not too low temperatures;[29] and we consider quasielastic scattering, with $\varepsilon_{\mathbf{k}},\varepsilon_{\mathbf{k}'}\gg\hbar\omega_{\mathbf{q}}$. The linearized collision integral then reads as

$$\begin{aligned}\delta\dot{f}_{\mathbf{k}}|_{\text{scatt}} &= -\frac{2\pi}{\hbar}\sum_{\mathbf{k}'}\sum_{\mathbf{q},\nu} w_{\nu}(\mathbf{q},\mathbf{k},\mathbf{k}')\omega_{\mathbf{q}}^{\nu}\frac{\partial n_{\mathbf{q}}}{\partial\omega_{\mathbf{q}}^{\nu}}\frac{\partial f_{\mathbf{k}}^{(0)}}{\partial\epsilon_{\mathbf{k}}}\\ &\times(\varphi_{\mathbf{k}}-\varphi_{\mathbf{k}'})\delta_{\mathbf{k},\mathbf{k}'+\mathbf{q}}\delta(\epsilon_{\mathbf{k}}-\epsilon_{\mathbf{k}'}),\end{aligned}\tag{A12}$$

so Eq. (A12) can be put in the form of Eq. (27):

$$\dot{f}_{\mathbf{k}}|_{\text{scatt}}=-\sum_{\mathbf{k}'}\mathcal{P}_{\mathbf{k},\mathbf{k}'}(\varphi_{\mathbf{k}}-\varphi_{\mathbf{k}'}),\tag{A13}$$

where $\mathcal{P}_{\mathbf{k},\mathbf{k}'}$ is given in Eq. (32).

Now, we proceed with the linearization of the collision integral in Eq. (A8), originating from scattering processes involving two FPs. At equilibrium, detailed balance is guaranteed $\dot{f}_{\mathbf{k}}^{(0)}|_{\text{scatt}}=0$, and the following two relations hold:

$$\begin{aligned}\frac{f_{\mathbf{k}'}^{(0)}}{1-f_{\mathbf{k}'}^{(0)}} &= \frac{f_{\mathbf{k}}^{(0)}}{1-f_{\mathbf{k}}^{(0)}}\frac{n_{\mathbf{q}}^{(0)}}{n_{\mathbf{q}}^{(0)}+1}\frac{n_{\mathbf{q}'}^{(0)}}{n_{\mathbf{q}'}+1},\\ \frac{f_{\mathbf{k}'}^{(0)}}{1-f_{\mathbf{k}'}^{(0)}}\frac{n_{\mathbf{q}'}^{(0)}}{n_{\mathbf{q}'}^{(0)}+1} &= \frac{f_{\mathbf{k}}^{(0)}}{1-f_{\mathbf{k}}^{(0)}}\frac{n_{\mathbf{q}}^{(0)}}{n_{\mathbf{q}}^{(0)}+1}.\end{aligned}\tag{A14}$$

In order to get the linearized collision integral, it is easy to see that we only need the following two variations:

$$\delta[f_{\mathbf{k}'}(1-f_{\mathbf{k}})(n_{\mathbf{q}}+1)(n_{\mathbf{q}'}+1)-f_{\mathbf{k}}(1-f_{\mathbf{k}'})n_{\mathbf{q}}n_{\mathbf{q}'}]\tag{A15}$$

and

$$\delta[f_{\mathbf{k}'}(1-f_{\mathbf{k}})(n_{\mathbf{q}}+1)n_{\mathbf{q}'}-f_{\mathbf{k}}(1-f_{\mathbf{k}'})n_{\mathbf{q}}(n_{\mathbf{q}'}+1)],\tag{A16}$$

with the other two possibilities being related with these by a minus sign and $\mathbf{k}\to\mathbf{k}'$. After a similar calculation as in the one-phonon scattering case (see supplementary material for details[40]), these variations can be written in terms of the equilibrium distributions, its derivatives, and $\varphi_{\mathbf{k}}$, $\chi_{\mathbf{q}}$. Then, we introduce the two typical approximations: We consider phonons to be in equilibrium $\chi_{\mathbf{q}}\approx 0$, so that $n_{\mathbf{q}}\approx n_{\mathbf{q}}^{(0)}$, and we assume quasielastic scattering. The linearized collision integral then reads as

$$\begin{aligned}\delta\dot{f}_{\mathbf{k}}|_{\text{scatt}} &= -\frac{2\pi}{\hbar^2}k_BT\frac{\partial f_{\mathbf{k}}}{\partial\varepsilon_{\mathbf{k}}}\sum_{\mathbf{k}'}(\varphi_{\mathbf{k}'}-\varphi_{\mathbf{k}})\sum_{\mathbf{q},\mathbf{q}'}w_F(\mathbf{q},\mathbf{q}',\mathbf{k},\mathbf{k}')\\ &\times\left(\frac{\omega_{\mathbf{q}}^{F}+\omega_{\mathbf{q}'}^{F}}{1+n_{\mathbf{q}}+n_{\mathbf{q}'}}-\frac{\omega_{\mathbf{q}}^{F}-\omega_{\mathbf{q}'}^{F}}{n_{\mathbf{q}}-n_{\mathbf{q}'}}\right)\\ &\times\frac{\partial n_{\mathbf{q}}}{\partial\omega_{\mathbf{q}}^{F}}\frac{\partial n_{\mathbf{q}'}}{\partial\omega_{\mathbf{q}'}^{F}}\delta_{\mathbf{k},\mathbf{k}'+\mathbf{q}+\mathbf{q}'}\delta(\epsilon_{\mathbf{k}}-\epsilon_{\mathbf{k}'}),\end{aligned}\tag{A17}$$

It can be written in the form of Eq. (A13), with $\mathcal{P}_{\mathbf{k},\mathbf{k}'}$ as given in Eq. (33).

APPENDIX B: CALCULATING THE RESISTIVITY

In this appendix, we provide details regarding the calculation of the T-dependent resistivity for bilayer graphene. The variational method is used, with resistivity given by Eq. (36). By writing the numerator in Eq. (36) as in Eq. (37), the

resistivity can be cast in the form

$$\varrho = \frac{\mathcal{V}\hbar^2}{8\pi^2 e^2 k_F^4} \int d\mathbf{k}\, d\mathbf{k}'\, (\mathbf{K}\cdot\mathbf{u})^2\, \mathcal{P}_{\mathbf{k},\mathbf{k}'}\,. \tag{B1}$$

The remaining task is the calculation of the integral on the right-hand side of Eq. (B1).

1. Scattering by in-plane phonons

This case follows closely the derivation to the Bloch T^5 law in three-dimensional metals.[29] By inserting Eq. (32) for $\mathcal{P}_{\mathbf{k},\mathbf{k}'}$ into Eq. (B1), we get

$$\varrho = \frac{\mathcal{V}\hbar}{4\pi e^2 k_F^4} \int d\mathbf{k}\, d\mathbf{k}'\, (\mathbf{K}\cdot\mathbf{u})^2 \sum_\nu w_\nu(\mathbf{K},\mathbf{k},\mathbf{k}')\omega_{\mathbf{K}}^\nu \times \frac{\partial n_{\mathbf{K}}^{(0)}}{\partial\omega_{\mathbf{K}}^\nu} \frac{\partial f_{\mathbf{k}}^{(0)}}{\partial\epsilon_{\mathbf{k}}} \delta(\epsilon_{\mathbf{k}} - \epsilon_{\mathbf{k}'}), \tag{B2}$$

where we have already performed the sum over $\mathbf{q}$. We can simplify the integral above by integrating over k and k' noting the presence of $\delta(\epsilon_{\mathbf{k}} - \epsilon_{\mathbf{k}'})$ and $\frac{\partial f_{\mathbf{k}}}{\partial\epsilon_{\mathbf{k}}} \approx -\delta(\epsilon_F - \epsilon_{\mathbf{k}})$. The result reads as

$$\varrho \approx -\frac{\mathcal{V}\hbar}{4\pi e^2 k_F^4} \left(\frac{m}{\hbar^2}\right)^2 \int d\theta_{\mathbf{k}} d\theta_{\mathbf{k}'}\, (\mathbf{K}\cdot\mathbf{u})^2 \times \sum_\nu w_\nu(\mathbf{K},k_F\hat{e}_{\mathbf{k}},k_F\hat{e}_{\mathbf{k}'})\omega_{\mathbf{K}}^\nu \frac{\partial n_{\mathbf{K}}^{(0)}}{\partial\omega_{\mathbf{K}}^\nu}, \tag{B3}$$

with $\mathbf{K} = k_F(\hat{e}_{\mathbf{k}} - \hat{e}_{\mathbf{k}'})$. In order to proceed with the calculation, we have to specify the kernel $w_\nu(\mathbf{K},k_F\hat{e}_{\mathbf{k}},k_F\hat{e}_{\mathbf{k}'})$ given in Eq. (34). By making use of the matrix elements in Eq. (23), we get

$$w_\nu(\mathbf{K},k_F\hat{e}_{\mathbf{k}},k_F\hat{e}_{\mathbf{k}'}) \equiv w_\nu(K) = \frac{\left[D_B^\nu(K/k_F)\right]^2 \hbar^3 k_F^2 K^2}{2\mathcal{V}\rho v_F^2 m^2 \omega_K^\nu}, \tag{B4}$$

with $D_B^\nu(x)$ as given in Eq. (43), and where we have used the relation $K = 2k_F \sin(\theta_{\mathbf{k},\mathbf{k}'}/2)$. The kernel depends only on $\theta_{\mathbf{k},\mathbf{k}'}$ or, equivalently, K (the norm of $\mathbf{K}$), as is the case of the rest of the factors in the integrand of Eq. (B3) but for $(\mathbf{K}\cdot\mathbf{u})^2$. The latter can be written as $(\mathbf{K}\cdot\mathbf{u})^2 = K^2\cos^2\gamma$, and the angular integration is then conveniently done by integrating over γ, keeping $\theta_{\mathbf{k},\mathbf{k}'} = \theta_{\mathbf{k}} - \theta_{\mathbf{k}'} \equiv \theta$ constant, and integrate over θ afterward, or equivalently K. By using $d\theta = dK/\sqrt{k_F^2 - K^2/4}$, the resistivity becomes

$$\varrho \approx -\frac{\mathcal{V}m^2}{2\hbar^3 e^2 k_F^4} \sum_\nu \int_0^{2k_F} dK\, \frac{K^2 w_\nu(K)\omega_K^\nu}{\sqrt{k_F^2 - K^2/4}} \frac{\partial n_K^{(0)}}{\partial\omega_K^\nu}. \tag{B5}$$

By inserting Eq. (B4) for the kernel $w_\nu(K)$ into Eq. (B5), we readily obtain Eq. (42). From this, it is straightforward to calculate analytically the two limiting cases $T \ll T_{\mathrm{BG}}$ and $T \gg T_{\mathrm{BG}}$.[29]

2. Scattering by flexural phonons

By inserting Eq. (33) for $\mathcal{P}_{\mathbf{k},\mathbf{k}'}$ into Eq. (B1), we get

$$\varrho = -\frac{\mathcal{V}k_B T}{4\pi e^2 k_F^4} \int d\mathbf{k}\, d\mathbf{k}'\, (\mathbf{K}\cdot\mathbf{u})^2 \times \sum_{\mathbf{q}} w_F(\mathbf{q},\mathbf{K}-\mathbf{q},\mathbf{k},\mathbf{k}') \frac{\partial n_{\mathbf{q}}}{\partial\omega_{\mathbf{q}}^F} \frac{\partial n_{\mathbf{q}'}}{\partial\omega_{\mathbf{q}'}^F} \frac{\partial f_{\mathbf{k}}^{(0)}}{\partial\varepsilon_{\mathbf{k}}} \delta(\varepsilon_{\mathbf{k}} - \varepsilon_{\mathbf{k}'}) \times \left(\frac{\omega_{\mathbf{q}}^F + \omega_{\mathbf{K}-\mathbf{q}}^F}{1 + n_{\mathbf{q}} + n_{\mathbf{K}-\mathbf{q}}} - \frac{\omega_{\mathbf{q}}^F - \omega_{\mathbf{K}-\mathbf{q}}^F}{n_{\mathbf{q}} - n_{\mathbf{K}-\mathbf{q}}}\right), \tag{B6}$$

where we have already performed the sum over $\mathbf{q}'$. We can simplify the integral above by integrating over k and k', noting the presence of $\delta(\epsilon_{\mathbf{k}} - \epsilon_{\mathbf{k}'})$ and $\frac{\partial f_{\mathbf{k}}}{\partial\epsilon_{\mathbf{k}}} \approx -\delta(\epsilon_F - \epsilon_{\mathbf{k}})$. The result reads as

$$\varrho \approx \frac{\mathcal{V}k_B T}{4\pi e^2 k_F^4} \left(\frac{m}{\hbar^2}\right)^2 \int d\theta_{\mathbf{k}} d\theta_{\mathbf{k}'}\, (\mathbf{K}\cdot\mathbf{u})^2 \times \sum_{\mathbf{q}} w_F(\mathbf{q},\mathbf{K}-\mathbf{q},k_F\hat{e}_{\mathbf{k}},k_F\hat{e}_{\mathbf{k}'}) \frac{\partial n_{\mathbf{q}}}{\partial\omega_{\mathbf{q}}^F} \frac{\partial n_{\mathbf{K}-\mathbf{q}}}{\partial\omega_{\mathbf{K}-\mathbf{q}}^F} \times \left(\frac{\omega_{\mathbf{q}}^F + \omega_{\mathbf{K}-\mathbf{q}}^F}{1 + n_{\mathbf{q}} + n_{\mathbf{K}-\mathbf{q}}} - \frac{\omega_{\mathbf{q}}^F - \omega_{\mathbf{K}-\mathbf{q}}^F}{n_{\mathbf{q}} - n_{\mathbf{K}-\mathbf{q}}}\right). \tag{B7}$$

The kernel $w_F(\mathbf{q},\mathbf{K}-\mathbf{q},k_F\hat{e}_{\mathbf{k}},k_F\hat{e}_{\mathbf{k}'})$ is given by Eq. (34) with $V_{\mathbf{q}}^\nu \to V_{\mathbf{q},\mathbf{q}'}^F$ (see Appendix A for a derivation). By inserting the matrix elements in Eq. (23), it takes the explicit form

$$w_F(\mathbf{q},\mathbf{K}-\mathbf{q},k_F\hat{e}_{\mathbf{k}},k_F\hat{e}_{\mathbf{k}'}) \equiv w_F(q,K,|\mathbf{K}-\mathbf{q}|) = \frac{\left[D_B^F(K/k_F)\right]^2 \hbar^4 q^2 k_F^2 |\mathbf{K}-\mathbf{q}|^2}{2^4\mathcal{V}^2 m^2 \rho^2 v_F^2 \omega_q^F \omega_{|\mathbf{K}-\mathbf{q}|}^F}, \tag{B8}$$

with $D_B^F(x)$ as given in Eq. (50), and where we have used the relation $K = 2k_F \sin(\theta_{\mathbf{k},\mathbf{k}'}/2)$ and assumed $\omega_{\mathbf{q}}^F$ given by Eq. (8). In deriving Eq. (B8), we used $\cos^2(\phi - \phi') = [1 + \cos(2\phi - 2\phi')]/2$ and dropped the oscillatory part. The sum over $\mathbf{q}$ can be replaced by an integral $\sum_{\mathbf{q}} \to \frac{\mathcal{V}}{(2\pi)^2}\int q\, dq\, d\phi$, and owing to the relation $Q^2 \equiv |\mathbf{K}-\mathbf{q}|^2 = K^2 + q^2 - 2qK\cos\phi$, we can write the resistivity as

$$\varrho \approx \frac{\mathcal{V}^2 k_B T}{8\pi^3 e^2 k_F^4} \left(\frac{m}{\hbar^2}\right)^2 \int d\theta_{\mathbf{k}} d\theta_{\mathbf{k}'}\, (\mathbf{K}\cdot\mathbf{u})^2 \int_0^\infty dq\, q \frac{\partial n_q}{\partial\omega_q^F} \times \int_{|K-q|}^{|K+q|} dQ\, \frac{Q w_F(q,K,Q)}{\sqrt{q^2K^2 - (K^2+q^2-Q^2)^2/4}} \frac{\partial n_Q}{\partial\omega_Q^F} \times \left(\frac{\omega_q^F + \omega_Q^F}{1 + n_q + n_Q} - \frac{\omega_q^F - \omega_Q^F}{n_q - n_Q}\right), \tag{B9}$$

where we used $d\phi = dQ\, Q/\sqrt{q^2K^2 - (K^2+q^2-Q^2)^2/4}$. As in Sec. B1, the angular integration over $\theta_{\mathbf{k}}$ and $\theta_{\mathbf{k}'}$ is conveniently done by integrating over γ, with $(\mathbf{K}\cdot\mathbf{u})^2 = K^2\cos^2\gamma$, keeping $\theta_{\mathbf{k},\mathbf{k}'} = \theta_{\mathbf{k}} - \theta_{\mathbf{k}'} \equiv \theta$ and q and $|\mathbf{K}-\mathbf{q}| \equiv Q$ constant, and integrate over θ afterward, q and Q. The resistivity may then be written as

$$\varrho \approx \frac{k_B T}{2^6\pi^2 e^2 \rho^2 v_F^2 k_F^2} \int_0^{2k_F} dK\, \frac{\left[D_B^F(K/k_F)\right]^2 K^2}{\sqrt{k_F^2 - K^2/4}} \times \int_0^\infty dq\, \frac{q^3}{\omega_q^F} \frac{\partial n_q}{\partial\omega_q^F} \int_{|K-q|}^{|K+q|} dQ \times \frac{Q^3}{\omega_Q^F \sqrt{q^2K^2 - (K^2+q^2-Q^2)^2/4}}$$

$$\times \frac{\partial n_Q}{\partial \omega_Q^F}\left(\frac{\omega_q^F+\omega_Q^F}{1+n_q+n_Q}-\frac{\omega_q^F-\omega_Q^F}{n_q-n_Q}\right), \tag{B10}$$

where $d\theta = dK/\sqrt{k_F^2-K^2/4}$ has been used, and we used Eq. (B10) for the kernel.

a. Nonstrained flexural phonons

In the absence of strain, the FP dispersion reads as $\omega_q^F = \alpha q^2$. After rescaling momentum as $x \to \tilde{x} = x(\hbar\alpha/k_BT)^{1/2}$, we can rewrite the resistivity as

$$\begin{aligned}\varrho \approx{}& \frac{(k_BT)^2}{2^6\pi^2\hbar e^2\rho^2 v_F^2 k_F^2\alpha^4}\int_0^{2\tilde{k}_F} d\tilde{K}\,\frac{\left[D_B^F(\tilde{K}/\tilde{k}_F)\right]^2\tilde{K}^2}{\sqrt{\tilde{k}_F^2-\tilde{K}^2/4}}\\ &\times\int_0^\infty d\tilde{q}\,\tilde{q}n_{\tilde{q}}(n_{\tilde{q}}+1)\int_{|\tilde{K}-\tilde{q}|}^{|\tilde{K}+\tilde{q}|}d\tilde{Q}\\ &\times\frac{\tilde{Q}n_{\tilde{Q}}(n_{\tilde{Q}}+1)}{\sqrt{\tilde{q}^2\tilde{K}^2-(\tilde{K}^2+\tilde{q}^2-\tilde{Q}^2)^2/4}}\\ &\times\left(\frac{\tilde{q}^2+\tilde{Q}^2}{1+n_{\tilde{q}}+n_{\tilde{Q}}}-\frac{\tilde{q}^2-\tilde{Q}^2}{n_{\tilde{q}}-n_{\tilde{Q}}}\right).\end{aligned} \tag{B11}$$

The integral over $\tilde{Q}$ is infrared divergent, and is thus dominated by the contribution $\tilde{K}\sim\tilde{q}$. By defining the small quantity $\delta x = |\tilde{K}-\tilde{q}|$, and noting that, for $\tilde{Q}\ll 1$, we have $n_{\tilde{Q}}\sim 1/\tilde{Q}^2\gg 1$, it is possible to identify the dominant contribution in the $\tilde{Q}$ integral as

$$\begin{aligned}&\int_{|\tilde{K}-\tilde{q}|}^{|\tilde{K}+\tilde{q}|}d\tilde{Q}\,\frac{\tilde{Q}n_{\tilde{Q}}(n_{\tilde{Q}}+1)}{\sqrt{\tilde{q}^2\tilde{K}^2-(\tilde{K}^2+\tilde{q}^2-\tilde{Q}^2)^2/4}}\\ &\quad\times\left(\frac{\tilde{q}^2+\tilde{Q}^2}{1+n_{\tilde{q}}+n_{\tilde{Q}}}-\frac{\tilde{q}^2-\tilde{Q}^2}{n_{\tilde{q}}-n_{\tilde{Q}}}\right)\\ &\quad\sim 2\tilde{K}^2\int_{\delta x}^{2\tilde{K}}d\tilde{Q}\,\frac{n_{\tilde{Q}}+1}{\tilde{K}}\sim\frac{2\tilde{K}}{\delta x}.\end{aligned}$$

It is now obvious that the $\tilde{q}$ integral has a logarithmic divergence for $\tilde{q}\sim\tilde{K}$. Note, however, that in the present theory, phonons have an infrared cutoff, so that $\min|\tilde{K}-\tilde{q}| = \tilde{q}_c$, where $\tilde{q}_c\ll 1$ is either due to strain or anharmonic effects. The dominant contribution to the $\tilde{q}$ integral is then coming from the maximum of $1/|\tilde{K}-\tilde{q}|$, from which we obtain

$$\begin{aligned}&2\tilde{K}\int_0^\infty d\tilde{q}\,\tilde{q}n_{\tilde{q}}(n_{\tilde{q}}+1)\frac{1}{|\tilde{q}-\tilde{K}|}\\ &\quad\sim -2\pi\tilde{K}^2 n_{\tilde{K}}(n_{\tilde{K}}+1)\ln(\tilde{q}_c).\end{aligned}$$

The resistivity may finally be written as a simple integral over $\tilde{K}$,

$$\begin{aligned}\varrho \approx{}& \frac{(k_BT)^2}{2^6\pi\hbar e^2\rho^2 v_F^2 k_F^2\alpha^4}\ln\left(\frac{k_BT}{\hbar\alpha q_c^2}\right)\\ &\times\int_0^{2\tilde{k}_F}d\tilde{K}\,\frac{[D(\tilde{K}/\tilde{k}_F)]^2}{\sqrt{\tilde{k}_F^2-\tilde{K}^2/4}}\tilde{K}^4 n_{\tilde{K}}(n_{\tilde{K}}+1),\end{aligned} \tag{B12}$$

from which Eq. (49) is readily obtained.

b. Strained flexural phonons

The flexural phonon dispersion in the isotropic approximation is $\omega_q^F\approx\sqrt{\alpha^2q^4+\bar{u}v_L^2q^2}$ [see Eq. (8)]. After rescaling momenta $x\to\tilde{x} = x\hbar v_L u^{1/2}/(k_BT)$, the resistivity in Eq. (B10) takes the form given in Eq. (56). The low-T regime is detailed in the main text. Here, we concentrate in the high-T regime, showing in particular how to obtain Eq. (60) for the integrals over $\tilde{q}$ and $\tilde{Q}$ in Eq. (56).

We start by writing the $\tilde{Q}$ integral in Eq. (56) as

$$\begin{aligned}&\mathcal{I}(\gamma,\tilde{K},\tilde{q})\\ &\equiv\int_{|\tilde{K}-\tilde{q}|}^{|\tilde{K}+\tilde{q}|}d\tilde{Q}\,\frac{\tilde{Q}^3n_{\tilde{Q}}(n_{\tilde{Q}}+1)}{\sqrt{\tilde{q}^2\tilde{K}^2-(\tilde{K}^2+\tilde{q}^2-\tilde{Q}^2)^2/4}}\\ &\quad\times\frac{1}{\sqrt{\gamma^2\tilde{Q}^4+\tilde{Q}^2}}\left(\frac{\sqrt{\gamma^2\tilde{q}^4+\tilde{q}^2}+\sqrt{\gamma^2\tilde{Q}^4+\tilde{Q}^2}}{1+n_{\tilde{q}}+n_{\tilde{Q}}}\right.\\ &\quad\left.-\frac{\sqrt{\gamma^2\tilde{q}^4+\tilde{q}^2}-\sqrt{\gamma^2\tilde{Q}^4+\tilde{Q}^2}}{n_{\tilde{q}}-n_{\tilde{Q}}}\right),\end{aligned} \tag{B13}$$

with $\gamma=\sqrt{2}\omega_{q_T}^F/\omega_{q^*}^F$. Having in mind that high T implies $\tilde{K}\ll 1$, we consider the integration in Eq. (B13) in two limiting cases: when $\tilde{q}\lesssim\tilde{K}\ll 1$ and for $\tilde{q}\gg\tilde{K}$. In the former case, since $\tilde{q}\ll 1$ and $\tilde{Q}\ll 1$ hold, we can linearize the dispersion relation and approximate the Bose-Einstein distribution function by $n_{\tilde{q}}\approx 1/\tilde{q}$ and $n_{\tilde{Q}}\approx 1/\tilde{Q}$ (as discussed in the main text, finite strain implies $k_F\ll q^*$, so that the linearization of the flexural phonon dispersion can be taken when $\tilde{q}\lesssim\tilde{K}\ll 1$ holds). The integral over $\tilde{Q}$ in Eq. (B13) may then be approximated by

$$\begin{aligned}\mathcal{I}(\gamma,\tilde{K},\tilde{q})\approx{}&\int_{|\tilde{K}-\tilde{q}|}^{|\tilde{K}+\tilde{q}|}d\tilde{Q}\\ &\times\frac{2\tilde{q}\tilde{Q}}{\sqrt{\tilde{q}^2\tilde{K}^2-(\tilde{K}^2+\tilde{q}^2-\tilde{Q}^2)^2/4}},\end{aligned} \tag{B14}$$

and the integral can be done as

$$\begin{aligned}\mathcal{I}(\gamma,\tilde{K},\tilde{q})\approx{}&\int_{|\tilde{K}-\tilde{q}|}^{|\tilde{K}+\tilde{q}|}d\tilde{Q}\,\frac{4\tilde{q}\tilde{Q}}{\sqrt{Y(\tilde{q},\tilde{Q},\tilde{K})}}\\ ={}&2\tilde{q}\arctan\left[\frac{\tilde{q}^2+\tilde{K}^2-\tilde{Q}^2}{\sqrt{Y(\tilde{q},\tilde{Q},\tilde{K})}}\right]_{|\tilde{K}-\tilde{q}|}^{|\tilde{K}+\tilde{q}|}\\ ={}&2\pi\tilde{q}\equiv\mathcal{I}(\tilde{q}),\end{aligned} \tag{B15}$$

where we have defined

$$\begin{aligned}Y(\tilde{q},\tilde{Q},\tilde{K}) ={}&-(\tilde{q}-\tilde{K}-\tilde{Q})(\tilde{q}-\tilde{K}+\tilde{Q})\\ &\times(\tilde{q}+\tilde{K}-\tilde{Q})(\tilde{q}+\tilde{K}+\tilde{Q}).\end{aligned}$$

On the other hand, for $\tilde{q}\gg\tilde{K}$, the integration region is concentrated around $\tilde{q}$. We may then write the integral in Eq. (B13) as a slowly varying function, which we can take out of the integral, multiplied by an integral of the form of that in Eq. (B14):

$$\mathcal{I}(\gamma,\tilde{K},\tilde{q})\approx\frac{\tilde{q}^2n_{\tilde{q}}(n_{\tilde{q}}+1)}{\sqrt{\gamma^2\tilde{q}^4+\tilde{q}^2}}\left(\frac{2\sqrt{\gamma^2\tilde{q}^4+\tilde{q}^2}}{1+2n_{\tilde{q}}}+\frac{1}{n_{\tilde{q}}(n_{\tilde{q}}+1)}\right)$$

$$\times \int_{|\tilde{K}-\tilde{q}|}^{|\tilde{K}+\tilde{q}|} d\tilde{Q}\, \frac{\tilde{Q}}{\sqrt{\tilde{q}^2\tilde{K}^2-(\tilde{K}^2+\tilde{q}^2-\tilde{Q}^2)^2/4}}$$
$$\approx \frac{\pi\tilde{q}^2 n_{\tilde{q}}(n_{\tilde{q}}+1)}{\sqrt{\gamma^2\tilde{q}^4+\tilde{q}^2}}\left(\frac{2\sqrt{\gamma^2\tilde{q}^4+\tilde{q}^2}}{1+2n_{\tilde{q}}}+\frac{1}{n_{\tilde{q}}(n_{\tilde{q}}+1)}\right)$$
$$\equiv \mathcal{I}(\gamma,\tilde{q}). \quad \text{(B16)}$$

Since, for $\tilde{q} \lesssim \tilde{K}$, the latter result reduces to $2\pi\tilde{q}$, as in Eq. (B15), we can use $\mathcal{I}(\gamma,\tilde{q})$ in Eq. (B16) to approximate the $\tilde{Q}$ integral [Eq. (B13)] in the full region $\tilde{q} \lesssim \tilde{K} \ll 1$ to $\tilde{q} \gg \tilde{K}$. This has been tested numerically to be a good approximation, as long as $\tilde{K} \ll 1$. The $\tilde{q}$ integral in Eq. (56) may then be cast in the $\tilde{K}$-independent form given in Eq. (60).

[1] B. E. Feldman, J. Martin, and A. Yacoby, Nat. Phys. **5**, 889 (2009).
[2] Y. Zhang, T.-T. Tang, C. Girit, Z. Hao, M. C. Martin, A. Zettl, M. F. Crommie, Y. R. Shen, and F. Wang, Nature (London) **459**, 820 (2009).
[3] K. I. Bolotin, K. J. Sikes, Z. Jiang, G. Fudenberg, J. Hone, P. Kim, and H. L. Stormer, Solid State Commun. **146**, 351 (2008).
[4] X. Du, I. Skachko, A. Barker, and E. Y. Andrei, Nat. Nanotechnol. **3**, 491 (2008).
[5] S. V. Morozov, K. S. Novoselov, M. I. Katsnelson, F. Schedin, D. Elias, J. A. Jaszczak, and A. K. Geim, Phys. Rev. Lett. **100**, 016602 (2008).
[6] E. V. Castro, H. Ochoa, M. I. Katsnelson, R. V. Gorbachev, D. C. Elias, K. S. Novoselov, A. K. Geim, and F. Guinea, Phys. Rev. Lett. **105**, 266601 (2010).
[7] E. Mariani and F. von Oppen, Phys. Rev. B **82**, 195403 (2010).
[8] H. Ochoa, E. V. Castro, M. I. Katsnelson, and F. Guinea, Physica E e-print arXiv:1008.2523v1.
[9] W. Bao, F. Miao, Z. Chen, H. Zhang, W. Jang, C. Dames, and C. N. Lau, Nat. Nanotechnol. **4**, 562 (2009).
[10] C. Chen, S. Rosenblatt, K. I. Bolotin, W. Kalb, P. Kim, I. Kymissis, H. L. Stormer, T. F. Heinz, and J. Hone, Nature Nanotech **4**, 861 (2009).
[11] A. H. Castro Neto, F. Guinea, N. M. R. Peres, K. S. Novoselov, and A. K. Geim, Rev. Mod. Phys. **81**, 109 (2009).
[12] K. V. Zakharchenko, M. I. Katsnelson, and A. Fasolino, Phys. Rev. Lett. **102**, 046808 (2009).
[13] L. D. Landau and E. M. Lifshitz, *Theory of Elasticity* (Pergamon, Oxford, 1970).
[14] *Statistical Mechanics of Membranes and Surfaces*, edited by D. Nelson, T. Piran, and S. Weinberg (World Scientific, New Jersey, 2004).
[15] K. N. Kudin, G. E. Scuseria, and B. I. Yakobson, Phys. Rev. B **64**, 235406 (2001).
[16] C. Lee, X. Wei, J. W. Kysar, and J. Hone, Science **321**, 385 (2008).
[17] K. V. Zakharchenko, J. H. Los, M. I. Katsnelson, and A. Fasolino, Phys. Rev. B **81**, 235439 (2010).
[18] E. Mariani and F. von Oppen, Phys. Rev. Lett. **100**, 076801 (2008).
[19] M. M. Fogler, F. Guinea, and M. I. Katsnelson, Phys. Rev. Lett. **101**, 226804 (2008).
[20] H. Suzuura and T. Ando, Phys. Rev. B **65**, 235412 (2002).
[21] S.-M. Choi, S.-H. Jhi, and Y.-W. Son, Phys. Rev. B **81**, 081407(R) (2010).
[22] S. V. Morozov, K. S. Novoselov, M. I. Katsnelson, F. Schedin, L. A. Ponomarenko, D. Jiang, and A. K. Geim, Phys. Rev. Lett. **97**, 016801 (2006).
[23] M. Katsnelson and K. Novoselov, Solid State Commun. **143**, 3 (2007).
[24] M. I. Katsnelson and A. K. Geim, Philos. Trans. R. Soc., A **366**, 195 (2008).
[25] F. Guinea, B. Horovitz, and P. Le Doussal, Phys. Rev. B **77**, 205421 (2008).
[26] A. Altland and B. Simons, *Condensed Matter Field Theory* (Cambridge University, Cambridge, 2006).
[27] M. Auslender and M. I. Katsnelson, Phys. Rev. B **76**, 235425 (2007).
[28] E. Cappelluti and L. Benfatto, Phys. Rev. B **79**, 035419 (2009).
[29] J. M. Ziman, *Electrons and Phonons: The Theory of Transport Phenomena in Solids* (Oxford Univesity, London, 1960).
[30] The fact that scattering is elastic and the Fermi surface isotropic makes unimportant factors depending only on k, the absolute value of momentum.
[31] V. Y. Irkhin and M. I. Katsnelson, Eur. Phys. J. B **30**, 481 (2002).
[32] H. Min, E. H. Hwang, and S. Das Sarma, Phys. Rev. B **83**, 161404(R) (2011).
[33] E. H. Hwang and S. Das Sarma, Phys. Rev. B **77**, 115449 (2008).
[34] T. Stauber, N. M. R. Peres, and F. Guinea, Phys. Rev. B **76**, 205423 (2007).
[35] J. H. Chen, C. Jang, S. Xiao, M. Ishigami, and M. S. Fuhrer, Nat. Nanotechnol. **3**, 206 (2008).
[36] D. K. Efetov and P. Kim, Phys. Rev. Lett. **105**, 256805 (2010).
[37] A. Cano, Phys. Rev. B **79**, 153410 (2009).
[38] K. V. Zakharchenko, R. Roldan, A. Fasolino, and M. I. Katsnelson, Phys. Rev. B **82**, 125435 (2010).
[39] R. Roldán, A. Fasolino, K. V. Zakharchenko, and M. I. Katsnelson, Phys. Rev. B **83**, 174104(R) (2011).
[40] See supplemental material at [http://link.aps.org/supplemental/10.1103/PhysRevB.83.235416].
[41] L. D. Landau and E. M. Lifshitz, *Physical Kinetics* (Pergamon, Oxford, 1981).